N O T I C E

THIS DOCUMENT HAS BEEN REPRODUCED FROM MICROFICHE. ALTHOUGH IT IS RECOGNIZED THAT CERTAIN PORTIONS ARE ILLEGIBLE, IT IS BEING RELEASED IN THE INTEREST OF MAKING AVAILABLE AS MUCH INFORMATION AS POSSIBLE

NASA

Technical Memorandum 82036

Magnetic Field Directional Discontinuities : 2. Characteristics Between 0.46 and 1.0 AU

R. P. Lepping,
K.W. Behannon

NOVEMBER 1980

National Aeronautics and Space Administration
Goddard Space Flight Center
Greenbelt, Maryland 20771

MAGNETIC FIELD DIRECTIONAL DISCONTINUITIES: 2. CHARACTERISTICS BETWEEN 0.46 AND 1.0 AU

R. P. Lepping
K. W. Behannon
Goddard Space Flight Center
Laboratory for Extraterrestrial Physics
Greenbelt, Maryland 20771

September 1980

ABSTRACT

The characteristics of directional discontinuities (DD's) in the interplanetary magnetic field have been studied using data from the Mariner 10 primary mission between 1.0 and 0.46 AU during November 1973-April 1974. The entire data set was surveyed using an automated procedure to identify DD's as changes in field direction of at least 30° in a 42 sec interval. This study yielded an $r^{-1.3\pm0.4}$ heliographic distance dependence for the daily average number per hour of discontinuities. In addition to this statistical survey, DD's were visually identified using 1.2 sec averages for three selected time intervals, and the corresponding 40 msec data were studied in detail by means of the Sonnerup-Cahill minimum variance procedure. After editing there resulted a total of 644 events. Two methods were used to estimate the ratio of the number of tangential discontinuities (TD's) to the number of rotational discontinuities (RD's). In the first approach, those DD's with substantial normal components ($B_n/\langle B\rangle \geq 0.3$) were interpreted as RD's and the remainder were considered to be TD's, except that some "RD's" were eliminated on the basis of unacceptably large relative magnitude variances across their discontinuity zone. The second method considers the total number of RD's to be the sum of those DD's with substantial normal components (again excluding those with large variances) plus an estimated number of those DD's with small normal components that are possibly RD's. The estimate is based on the assumption that there is a uniform distribution of RD's per degree of discontinuity cone angle β ($= \cos^{-1}|B_n|/B$, where B is the average magnitude of the field across the DD) for all β. Then all other DD's are assumed to be TD's. Both methods show that the ratio of TD's to RD's varied with time and decreased with decreasing radial distance but was $\sim 1.2 \pm 0.3$ on average from the first method and $\sim 0.66 \pm 0.23$ on average from the second. A decrease in average discontinuity thickness of $\sim$40% was found between 1.0 and 0.72 AU and $\sim$ 54% between 1.0 and 0.46 AU, independent of type (TD or RD). This decrease in thickness for decreasing r is in qualitative agreement with Pioneer 10 observations between 1 and 5 AU. When the individual DD thicknesses are normalized with respect to the estimated local proton gyroradius (R_L), the average thickness at the three locations given above is nearly constant, $43 \pm 6\ R_L$. This also holds true for both

RD's and TD's separately. Statistical distributions of other properties, such as normal components and discontinuity-plane angles (ω), are presented. No obvious relationship was found between ω and the thickness of either TD's or RD's when widely separated locations are examined.

INTRODUCTION

Early investigations of the fine-scale variations of the interplanetary magnetic field (IMF) revealed occasional changes in the direction of the field that were abrupt on time scales of seconds (Ness et al., 1966). These features, termed directional discontinuities (DD's) by Burlaga (1969a), were defined by Burlaga to be changes in field direction of $> 30^{\circ}$ in ≤ 30 sec. Statistical studies (Siscoe et al., 1968; Burlaga, 1969a) have shown that DD's are observed near 1 AU at an average rate of $\sim$ 1/hour. The observed DD's have been identified as to type, i.e., either tangential or rotational discontinuities (TD's or RD's) (Smith, 1973a, b; Martin et al., 1973; Solodyna et al., 1977; Burlaga et al., 1977), with a predominance of TD's found in quiet, low-speed solar wind regions. Although plasma measurements are required in addition to the magnetic field measurements for absolute identification of DD type, most of the DD studies to date have used only magnetic field data, basing the identification of DD type on the magnitude of the field component normal to a plane which is estimated by analysis to be the plane of the discontinuity. Observing the discontinuities at two or more spacecraft locations can provide additional useful information (Denskat and Burlaga, 1977; Fitzenreiter, 1979).

The study of DD's in the IMF is important for the better understanding of fundamental plasma processes in the solar wind. RD's are limiting case Alfvenic fluctuations, essentially propagating kinks in the magnetic field, that are probably important as scatterers of cosmic ray particles. TD's, on the other hand, are surfaces separating adjacent plasma regions having differently directed fields and flow velocity and no components of $\vec{B}$ or $\vec{V}$ perpendicular to the surface in its frame of reference. Thus they are nonpropagating boundaries between different plasma regimes in the solar wind and as such are potential sites of instability. There are questions concerning both the origin and stability of such structures. Are they

produced near the sun and then convected to large heliocentric distances essentially unchanged, or are they produced at all distances in colliding solar wind stream regions? Are these processes different for RD's and TD's? In order to answer such questions, the occurrence rate of RD's and TD's separately as a function of both radial distance from the sun and location in azimuth relative to the positions of high-speed streams must be determined.

Investigations to date have found that in regions of enhanced solar wind speed, an increasing fraction of DD's exhibit the plasma properties of outwardly propagating RD's (Solodyna et al., 1977), with approximately equal numbers of RD's and TD's observed in fast streams at 1 AU (Burlaga et al., 1977; Neubauer and Barnstorf, 1980; Barnstorf 1980). The first opportunity to study the occurrence of DD's over a range of heliocentric distance was provided by Pioneer 6 (Burlaga, 1971). The distance range covered was limited to 0.83-0.98 AU, however, and variations in data coverage and quality with distance, together with temporal variability, made it difficult to accurately assess a radial dependence in occurrence rate. It was concluded that most if not all DD's originate closer to the sun than 0.82 AU and do not change appreciably over the distance range of the Pioneer 6 observations.

Observations by Pioneers 10 and 11 at heliocentric distances between 1 and 8.5 AU (Tsurutani and Smith, 1979) extended considerably the study of the properties of DD's as functions of radial distance. The rate of occurrence was found to vary substantially from day to day and from one solar rotation to the next. The latter slow modulation is indicative of a correlation with changing solar conditions. A clear decrease in the rate of occurrence with increasing radial distance was found, amounting to 25% per AU. It was interpreted, however, as being possibly only an apparent variation due to the failure of increasingly thicker DD's to satisfy the Tsurutani and Smith (1979) identification criteria. Results were interpreted to be consistent with the origination of DD's near the sun and subsequent convection outward by the solar wind, in agreement with the conclusion from the Pioneer 6 results.

The first opportunity to study DD characteristics over a wide range of radial distance inward from 1 AU toward the sun, which is the principal subject of this paper, was provided by the Mariner 10 spacecraft, which performed measurements of the IMF and solar wind between 1.0 and 0.46 AU during the period 3 November 1973 and 14 April 1974 (Behannon, 1976). The spacecraft carried a dual triaxial fluxgate magnetometer system which has been described in detail by Seek et al. (1977). The calibration techniques used for this experiment and the accuracy of the data are described elsewhere (Ness et al., 1974; Lepping et al., 1975). The Mariner 10 DD study consists of two major parts: (1) The determination of daily occurrence rate of DD's over the 5-1/2 month Mariner 10 primary mission period using a computer-automated procedure; and (2) an investigation of the statistical properties of DD's, including classification as RD's or TD's, at three different distances from the sun using fine-scale (40 ms) vector data and employing a minimum variance analysis. The study considers magnetic field data only; solar wind proton measurments were not performed on Mariner 10. The classification of a DD as an RD or TD has been guided by the results of an error analysis which included simulation studies. These results and their application to Mariner 10 have been discussed in detail by Lepping and Behannon (1980), henceforth referred to as Paper 1. Subsequent to the Mariner 10 mission, the region of space between 0.3 and 1 AU was surveyed by the Helios 1 and 2 spacecraft. In the Summary and Discussion section, we compare the Mariner 10 results with those from Helios (Neubauer and Barnstorf, 1980; Barnstorf, 1980), as well as with previous studies at 1 AU (Burlaga, 1971; Burlaga et al., 1977) and the Pioneer 10 and 11 results (Tsurutani and Smith 1979).

DD OCCURRENCE RATE: A SURVEY OF DATA

IMF data in the form of 42 s vector averages for the period 3 November 1973 to mid April 1974 were examined by a computer program for the automatic identification of DD's. For purposes of this survey a DD was defined as a change of at least 30° in field direction in 42 s. Various checking interrogations are performed in the program to aid in properly identifying the DD's so that waves with periods near 42 or 84 s are not mistakenly accepted as DD's, for example. A description of the program is

given by Sari (1972). Figure 1 gives the results of the automated survey in terms of the daily average of the number of DD's per hour as a function of R, the normalized heliocentric radial distance. Even though there is considerable scatter in the data, a clear increasing trend with decreasing heliocentric distance (r) is seen. A least squares fit to these data yields $N = N_o (r/R_o)^{-1.3\pm0.4}$ where $R_o = 1$ AU and $N_o = 1.25$. The generality of this expression for $0.46 \leq r \leq 1$ AU is not known; strictly it holds for the epoch considered, but possibly indicates the proper quantitative trend in general. No correction was made in this analysis for the azimuthal speed of the spacecraft, as has been implemented for the Helios analysis (Barnstorf, 1980). For Mariner 10, the effect on the data would have been at most only marginal right at perihelion.

Considerable structure can be seen in the occurrence rate data. Reference to the magnetic sector polarity pattern included across the top of the figure suggests strongly that at least some of the structure in the occurrence rate is related to the large-scale structure of the interplanetary medium during this time. A comparison of the discontinuity rate with the hourly average field magnitude suggests that the maximum counts generally occurred during the few days immediately following the passage of compressed fields at the leading edges of high speed streams.

That the DD occurrence rate observed by Mariner 10 is structured into a recurring pattern of variations which is related to the magnetic polarity and field magnitude patterns supports the earlier conclusions of Belcher and Davis (1971) and Ness et al. (1971) that the properties of the interplanetary microstructure are correlated with the large-scale solar wind stream structure. The latter study bases the association on the observations by Burlaga et al. (1969b) that magnetic field fluctuations with periods in the range 1 minute to 1 hour are related to the proton beta, together with observations of a rise in proton beta with rising flow speed. This leads to the expectation of quiet fields at low flow speeds and disturbed fields at high speeds. Belcher (1975) also has suggested that there may be a short-period "clumpiness" to the occurrence rate for a given type of discontinuity that is related to the large-scale structure. The Mariner 10 discontinuity data used in the automated preliminary survey

of this section were not separated by type, i.e., by RD or TD identification.

Also shown at the top of the figure is the heliographic latitude of the spacecraft during this mission. One could also argue in this case that the variation is one with latitude rather than distance. We feel, however, that it is less likely that the DD occurrence rate would have continuously increased so systematically in going from northern to southern latitudes.

STATISTICAL PROPERTIES OF DD'S

Magnetic field data in the form of 1.2 s averages taken during the separate periods 4-17 November, 5-12 February, and 3-10 April, corresponding to the heliocentric distances of 1.0, 0.72, and 0.46 AU, respectively, were visually surveyed and sets of candidate DD's identified. Use of a visual survey approach permitted a degree of flexibility in interpretation and quality assessment on a case by case basis that would require a high level of sophistication in an automated procedure. Furthermore, it avoided having the selection process deliberately rate-limited. Broader, slower structures than those permitted by the criteria of a direction change of $\geq 30^{\circ}$ in 30 s (or 42 s), for example, can be admitted when they appeared to differ from the more rapid directional variations only in time scale. Figure 2 includes examples of candidate discontinuities that were narrow (a) and broad (b) in time. In principle, transition durations up to one minute were allowed, but none exceeding 45 s were found. Also, none of the cases selected had a rate of variation that actually exceeded one degree per second, although in one case that rate was equaled (Figure 2). In addition, a few DD's with discontinuity angle $\omega < 30^{\circ}$ were also tentatively selected as candidates when they were exceedingly smooth and sharply defined.

Principal goals were to determine the type and radial dependence of the DD's. There existed a relatively stationary stream and magnetic sector pattern during the 0.72 and 0.46 AU observations, and there was an attempt to study the same regions of the corotating structure in each case. The 0.72 AU period was bounded at the start by the Venus encounter, thus making

the total time in that interval about half of that at 1.0 AU. At the other end, the 0.46 AU data period was limited by the end of the primary mission data coverage, and was approximately equal in length to the 0.72 AU period.

Initially 750 DD's were individually identified, all of which were subsequently analyzed by the Sonnerup-Cahill (1967) minimum variance method. This is a means of estimating the discontinuity plane normal ($\hat{n}$) along which the difference vectors ($\Delta\vec{B}_i$) within the discontinuity zone have minimum variation, where $\Delta\vec{B}_i = \vec{B}_i - \langle\vec{B}_i\rangle$, $i = 1, \ldots, N_{final}$, and where $\langle\vec{B}_i\rangle$ is the average field across the zone (see Figure 6 of Burlaga et al., 1977). In the case of an ideal TD, all of the $\vec{B}_i$'s lie in the discontinuity plane; this is not the case for an RD, which has a constant component normal to the discontinuity plane. For both types, $\Delta\vec{B}_i$ lies in the discontinuity plane. What separates the ideal definition from actuality in these definitions is the existence of field fluctuations near and within the DD that occur on time scales associated with the scale length of the DD itself but having magnitude changes usually small compared to the discontinuity component changes (see Paper 1).

The minimum variance analysis was applied to 40 ms field measurements, and for each event various characteristics of the discontinuity were estimated, such as:

B, the average field magnitude $\langle|\vec{B}|\rangle$ across the DD;

ω, the angle in the discontinuity plane from the first to last vector observed within the current sheet;

type, TD or RD;

τ, the thickness of the transition zone (i.e., the current sheet) along the $\hat{n}$-direction;

ϕ_N, the longitude of the DD normal, and

θ_N, the latitude of the DD normal in a spacecraft centered solar

equatorial plane coordinate system, where $\phi = 0^{\circ}$ is toward the sun and positive θ is "northward";

$|B_n|$, the absolute value of the average of the estimated normal component across the DD;

β, the discontinuity cone angle between the normal direction (defined as the $\hat{n}$-direction) and $\langle\vec{B}\rangle$; i.e., $\beta = \cos^{-1}(|B_n|/b)$;

σ_{Bn}, the rms deviation of the normal component across the DD;

λ_2/λ_3, the ratio of the intermediate to the minimum eigenvalue of the variance ellipsoid from the minimum variance analysis (see Sonnerup and Cahill, 1967); this ratio is a partial measure of how well the minimum variance plane is determined; and

σ_F, the rms deviation of the magnitude of the field across the DD.

The above quantities will be estimated and summarized in statistical distribution form separately, where applicable, for TD's and RD's and for the three locations: 1.0, 0.72, and 0.46 AU. Since unreasonably large errors in the estimate of the DD normals occur when $\omega < 30^{\circ}$ and/or $\lambda_2/\lambda_3 < 2.0$ (Paper 1), we consider only those cases where $\omega \geq 30^{\circ}$ and $\lambda_2/\lambda_3 \geq 2.0$, which decreases the 750 trial cases to 644 cases to be collectively studied.

Figure 3 shows the percent distributions of the resulting eigenvalue ratios for the three chosen locations, which are the minimum, maximum and mid-positions of the spacecraft in heliocentric radial distance (r) during the principal part of its mission. The three distributions are similar, approximating a portion of a normal curve, and showing that a small minority of cases lie above $\lambda_2/\lambda_3 = 10$. We see that the number of DD's per position increases rather markedly as r decreases, especially considering that 14, 7-1/3, and 8 days of data were inspected for r = 1.0, 0.72, and 0.46 AU, respectively. This finding is qualitatively consistent with the occurrence rate result from the automated survey described above.

Figure 4 gives the percent distributions of the relative normal component, $|B_n|/B$, for the three locations. Regardless of the fact that many more DD's occur at 0.46 than at 1.0 AU, the distributions are very similar. The discontinuity cone angle $\beta[= \cos^{-1}(|B_n|/B)]$ is also shown at the bottom of the figure. According to a DD simulation study (Paper 1) a reasonable value of β to use for separating discontinuities by type is 72.5° (or $|B_n|/B = 0.3$), with a ~95% probability that RD's lie to the right of that value ($\beta < 72.5^\circ$) for the Mariner 10 data set.

In this study we shall classify the DD's according to type by this criterion and study them separately, especially with respect to their r dependence. Notice that Figure 4 tells us that a maximum estimate of the ratio of TD's to RD's in the regions investigated was approximately unity (1.3, 1.2 and 0.79 at r = 1.0, 0.72 and 0.46 AU, respectively, within roughly the same recurrent sector region), i.e., if all events to the left of $\beta = 72.5$ are assumed to be TD's. It was found that the overall ratio of TD's to RD's (for the same assumption) increased for increasing r as the minimum allowed eigenvalue ratio λ_2/λ_3 was increased from 2 to 6, i.e., as we became more restrictive. This is, of course, unreasonably restrictive.

Another simple discriminator can be applied to help separate TD's and RD's which involves the change in field magnitude, or fluctuations in magnitude, across the discontinuity, as measured by σ_F/F defined in figure 5. The figure shows a scatter diagram of σ_F/F versus β for the 1.0 AU data. Ideally, RD's in a nearly thermally isotropic solar wind should have no field magnitude change across the transition zone. Hence, we choose to restrict RD's at 1.0 AU arbitrarily (based loosely on the σ_F/F distribution) to those with $\sigma_F/F \leq 0.09$; this upper bound is shown in Figure 5 as a horizontal line. The vertical line at $\beta = 72.5^\circ$ is the TD-RD separation line previously discussed. The top-left box (n = 10) contains "RD" cases which we will discard as being too poor in quality to retain. The bottom-left box (n = 62) consists of "clean" RD's, i.e., high quality cases. Likewise the top-right box (n = 29) consists of "clean" TD's, and bottom-right box (n = 62) is composed of a mixture of TD's and RD's, but probably predominantly TD's as previous study has shown, at least at 1 AU (Burlaga, 1971). If, for instance, the population of clean RD's is

distributed uniformly in β, as the figure seems to imply for $15^\circ \leq \beta \leq 72.5^\circ$ (and as the bottom panel of Figure 4 also shows, to a good approximation), then there are 1.08 RD's per degree of β. Based on this assumption for all β there is expected to be 19 RD's in the mixed (bottom-right) box, which is 31% of the total number of mixed cases.

In a later discussion of the relative numbers of RD's and TD's, we shall use the above estimate to specify a lower limit on the TD/RD ratio. For purposes of separately studying the statistical properties of the two types of discontinuities, however, we shall simply assume that all DD's with $\beta \geq 72.5^\circ$ are TD's, since we are unable to identify the specific DD's in the mixed set which are in fact RD's. It should, however, be kept in mind that some unknown fraction of these "mixed" DD's, possibly as large as 31% in the case of the 1 AU data, could in reality be RD's. This dilemma would not be resolved by excluding from consideration all cases falling within an "uncertainty band" of β centered on 72.5° or extending from $\beta = 72.5^\circ$ to some lower value. Since there is no a priori reason why RD's should have only low values of β, and the measurements suggest that they do not, such an exclusion of cases would most certainly discriminate against RD's and thus would bias the estimation of the relative numbers of each type. If the only objective is to study properties of RD's and TD's separately with no concern for relative abundances, then such an exclusion could produce sets which are more purely RD's or TD's. The purity of the TD set in particular will always be questionable, however. It should be noted that there is also a chance that a small number of cases falling into the lower left-hand box of Figure 5 could actually be TD's as a result of the effect of a variation in field magnitude within some of the DD's on the minimum variance analysis results (see Paper 1). Simulation studies have shown that a small fraction (no more than 2%) of the total cases in which TD's have been erroneously identified as RD's due to field magnitude variation can get through the λ_2/λ_3 and σ_F/F screening mechanisms to contaminate the results. Since the estimated number of cases involved is so small, we shall neglect this additional potential source of error in our statistical studies.

Figure 6 is similar to Figure 5 except that in this case r = 0.72 AU.

Here the upper bound on σ_F/F for clean RD's was chosen to be 0.055, i.e., the 0.72 AU RD-candidate set had slightly less magnitude variability than the 1 AU set. In most general respects Figure 5's comments hold for Figure 6 as well. Again, if RD's are distributed uniformly in β (justified over the domain $0 \leq \beta \leq 72.5^\circ$ by the center panel of Figure 4), there should be 27 (or 41%) in the mixed, bottom-right, box of Figure 6. Figure 7 shows comparable results for the 0.46 AU position, where there is estimated to be 42 RD's in the mixed box, i.e., 47%. Notice also that there was a larger proportion of large σ_F/F TD cases (arrows at top-right) than for the 1.0 or 0.72 AU sets, and the candidate RD's were intermediate in magnitude variability, where the clean RD upper bound on σ_F/F was chosen to be 0.07. If one calculates the ratio of the number of TD's (full set) to the number of clean RD's, one obtains 1.5, 1.2 and 0.86 for 1.0, 0.72 and 0.46 AU, respectively, indicating possibly a significant trend in radial occurrence rate with respect to type. This trend is qualitatively maintained even if only clean TD's and clean RD's are used, except each ratio is decreased by a factor of ~ 3, but this is probably not a reasonable means of estimating this ratio. When the upper limit estimates on the numbers of RD's are used (i.e., using assumption of uniform distribution of RD's per degree of β for all β), the respective ratios of TD's to RD's become 0.89, 0.66 and 0.43, lower than the first set by a factor of ~ 2, but maintaining approximately the same trend. [Notice that the assumption of a uniform distribution of RD's over β does not hold quite as well at 0.46 AU, as the top panel of Figure 4 indicates.] Of additional interest in this limiting case is the fact that the estimated number of TD's remains nearly constant at the three locations (N = 72, 76 and 78, respectively; although recall that the number of days at each location is different), so that most of the change in the ratio TD's to RD's with decreasing radial distance is caused by an increase in the number of RD's.

Figures 8 and 9 present the distributions of longitude (ϕ_N) and latitude (θ_N), respectively, of the DD normals with respect to type, location, and quality ("clean" or not). The figures also give the average field direction $\phi_{<\vec{B}>}$, $\theta_{<\vec{B}>}$, where the average was computed from the measurements within the DD transition zone for all of the events. Both the ϕ_N and θ_N distribution sets are rather broad, probably due to the

variability of the average field direction on a fine time scale, and therefore interpretation is difficult, but some salient features are worth mentioning. First, we discuss the ϕ_N distributions for the RD's. With the exception of the 1.0 AU set, the distributions peak near an average of the $\phi_{\langle\vec{B}\rangle}$'s and the radial directions, which is not unreasonable for the propagation direction of steepened Alfvén waves (Denskat and Burlaga, 1977; see also review by Behannon and Burlaga, 1980, and references therein). [That the "clean" peak in ϕ_N tends to shift clockwise for increasing r for the 0.46 and 0.72 AU cases is of questionable significance.] The exception at 1.0 AU may be due to a combination of some TD contamination plus poorer statistics than the other sets. The TD ϕ_N distributions are reasonably well behaved in that they tend to have peaks approximately perpendicular to $\phi_{\langle\vec{B}\rangle}$ with the puzzling exception of the clean TD set at 0.46 AU, which very likely is due to field variability for part of the set. Recall that ideally a TD normal must be perpendicular to its transition zone field.

The θ_N distributions are less interesting, showing mainly that they are approximately symmetric about the solar equatorial plane and usually symmetric about the $\theta_{\langle\vec{B}\rangle}$ direction for both types. The TD θ_N distributions, however, show a tendency to possess high (+/-) inclinations, i.e., they infrequently lie in a plane parallel to the solar equatorial plane; this is not as true for the RD distributions.

Distributions of ω, the discontinuity plane angle, are given in Figure 10 in the usual format. The broadness of the distributions is quite evident. The depletion of cases at small ω is obviously in part a selection effect whereby DD's with small ω's were either deliberately, or unconsiously ignored in the initial visual identification procedure. Therefore, the average ω's, $\langle\omega\rangle$, shown in the figure are of <u>relative</u> importance only. The RD's are "clean" cases and the TD's are all those DD's where $\beta \geq 72.5^\circ$. The most obvious property of these distributions is that for a given type $\langle\omega\rangle$ is independent of r. The 10° difference in $\langle\omega\rangle$ between the TD's and RD's is probably statistically significant. Consider, for example, the 1.0 AU case where RMS $\{\omega\}$ is 38.5° for RD's and 32.2° for TD's for $N_{RD} = 62$ and $N_{TD} = 91$ (See Table 1). This yields RMS/$\sqrt{N}$ = 4.9° and 3.4° for the RD's and TD's, respectively, or a net pythagorean mean

deviation of 6.0°, less than the 10° difference in $\langle\omega\rangle$. The net error for the 0.72 AU set is likewise 5.1° and for 0.46 AU it is 4.4° (See Table 3). The 10° difference in the $\langle\omega\rangle$'s is apparently due to the near absence of TD's with $150 \leq \omega \leq 180^{\circ}$, as compared to the RD distribution. There does not appear to be a simple explanation for this difference, unless it is associated with comparative errors in estimating ω for the different types. That is, for a true TD, or an RD that appears to be a TD (through error in the normal estimation), the ω-estimate will be accurate or underestimated. Conversely, for a TD that, through error, appears to be an RD an overestimated ω will occur. For an RD that can be identified as an RD, but with an inaccurate normal component, the estimated ω may be larger or smaller depending on the sign of the error on the normal component. The net effect would likely be the positive 10° (or whatever) difference shown in Figure 10. If this is the case, it is not noteworthy, but the consistent result for ω for the three locations is still thought provoking. It is not surprising that the most probable ω, ω_M and $\langle\omega\rangle$ are $\sim 80^{\circ}$ for the TD's, since TD's are most stable at $\omega = 90^{\circ}$ (Sen, 1963; Burlaga, 1969b), and if ω_M and $\langle\omega\rangle$ are on average underestimated by 10° or so, the results are in reasonable agreement with theory.

We now consider a more physically interesting property of the DD's, their thicknesses. In order to estimate the thickness of an interplanetary discontinuity, it is necessary to know: (1) the speed at which it is convected past the spacecraft, (2) the attitude of the discontinuity plane, i.e., its normal, (3) the passage interval, and (4) if an RD, the propagation velocity relative to the solar wind. The third entity is usually well-determined and the second is estimated, but with considerable error on occasion. Since solar wind proton data was not available on this mission, the solar wind speed was assumed to be 400 km/s at all three locations. This is a reasonable assumption, since the data sets were not associated with high speed regions. Also, the available results of Mariner 10 electron analysis lend support to this assumption (Scudder and Olbert, 1979). The relative speeds of propagating discontinuities (RD's) were also unknown, but expected to be quite small relative to bulk flow speed, and therefore were neglected in this study. The resulting discontinuity thickness distributions are shown in Figure 11. In all cases, the

thickness is the distance across the current sheet comprising the discontinuity transition zone in the direction normal to the discontinuity plane. Again the RD's are "clean" cases and the TD's are all those DD's where $\beta \geq 72.5^{\circ}$.

At a given location, $\langle\tau\rangle$ is similar for the TD and RD distributions; the slight differences are not statistically significant as Tables 1, 2, 3, row 3 indicate, when RMS/$\sqrt{N}$ is determined. The most marked feature of the distributions is the strong trend for $\langle\tau\rangle$ to increase with increasing radial distance independent of type: 1,200 km, 1,600 km, and 2,700 km for 0.46, 0.72 and 1.0 AU, respectively. Also when that small percentage of cases with $\tau > 56{,}000$ km are ignored, the TD distributions are, at all locations, narrower than the RD distributions, even though $\langle\tau\rangle$ is approximately equal for both types at a given location. The RD distribution at 1.0 AU is especially broad, possibly due in part to marginal statistics. The strong variation of thickness with radial distance from the sun obtained in this analysis could not have resulted artificially from our assumption of a constant solar wind speed throughout. Assuming 400 km/s to be correct at 1 AU, to force the observed effect the average speed would have had to have been 533 km/s at 0.72 AU and 900 km/s at 0.46 AU, for the same average thickness at the three locations. If, on the other hand, 400 km/s was the correct speed at 0.72 AU, average speeds of 300 km/s at 1 AU and 675 km/s at 0.46 AU would have been required. Such large-scale radial speed gradients are unrealistic. Smaller errors are undoubtedly introduced by our simple constant speed assumption. Specifically, use of an estimated constant speed, instead of the actual local speed for each DD, must be partially responsible for the broadness of the thickness distributions. However, accounting for such errors would not significantly alter the resulting average or most probable value for the thickness distributions.

Figure 11 shows that there is a decrease in average DD thickness of $\sim$ 40% between 1.0 and 0.72 AU, and $\sim$ 54% between 1.0 and 0.46 AU. This decrease of average thickness as r decreases is in qualitative agreement with Pioneer 10 observations between 1 and 8.5 AU (Tsurutani and Smith, 1979). When the thickness estimate is normalized with respect to the

estimated local proton gyroradius (R_L) for each event separately, however, the average thickness (τ_L) for each of the six distributions (i.e., for all r and both types) is nearly constant, 43 ± 6 R_L, as Tables 1, 2, and 3, row 4, indicate.

The estimate of the local gyroradius that was used in each case was computed from

$$R_L = \frac{m_p c}{e} \frac{V_T}{B} = (2 k m_p)^{1/2} \frac{c}{e} \frac{(T)^{1/2}}{B}$$

i.e., R_L = (constant) $\dfrac{(T)^{1/2}}{B}$,

where V was assumed to be the proton thermal speed, and where the proton mass, m_p, the speed of light, c, the unit of electron charge, e, and Boltzman's constant, k, as well as scaling factors, have all been absorbed into the constant factor. For the temperature, values from the one fluid model of Whang and Chang (1965) were used, ranging from 0.6×10^5 °K at 1 AU to 1.3×10^5 °K at 0.46 AU. The gyroradius correspondingly varies from 330/B to 480/B (in km) over the same range, where B is the average field magnitude in nT. For example, for B = 6 and 20 nT at 1 and 0.46 AU, respectively, values of R_L = 54 and 24 km are obtained for the two distances. Use of a different temperature model would obviously change the results to some extent, but since the temperature dependence of R_L is a weak one, the result is not changed appreciably. For example, by using the proton temperature distance dependence in the two fluid model of Hartle and Barnes (1970), a similar constancy in thickness (normalized by R_L) over the three locations was obtained as with the estimates based on the one-fluid model of Whang and Chang (1965).

Tables 1, 2 and 3 also give a statistical summary of other various relevant physical properties of the DD's according to r and type.

An attempt was made to find a possible relationship between discontinuity thickness τ and the size of the discontinuity angle ω. A

great deal of scatter in τ across the full range of ω was found at all three locations. The results are summarized in Figure 12 in the form of averages over 20° intervals of ω. The vertical bars associated with each of these mean values express the scatter (uncertainty) of the thickness data in that ω interval in terms of the standard deviation of the τ values about the mean divided by $\sqrt{N}$, where N is the number of values within the interval. As can be seen, no obvious general relationship exists between τ and ω.

SUMMARY AND DISCUSSION OF OBSERVATIONS

We provide here a brief summary of the results in the order that they were presented:

1. The average number of DD's per day decreases with increasing heliocentric distance (r), with large variability, and is approximately described by: Rate = $1.25\ r^{-1.28 \pm 0.4}$ (Figure 1).

2. To a first approximation the distributions of the ratios of intermediate to minimum eigenvalues (λ_2/λ_3) are normal and rather broad, and appear independent of r. (Figure 3).

3. The relative normal component (B_n/B) distributions are similar for the three locations of interest (i.e., at 1.0, 0.72 and 0.46 AU), and, for a simple partition value of $B_n/B = 0.3$, the ratio of the TD's to RD's for these locations is 1.3, 1.2 and 0.79, respectively (Figure 4).

4. When σ_F/F versus β is used in conjunction with $B_n/B = 0.3$ as a discriminator of TD's and RD's, the upper limit for the ratio of the number of TD's to the number of RD's becomes 1.5, 1.2, and 0.86 for 1.0, 0.72 and 0.46 AU respectively. (Figures 5, 6, 7). Assuming a uniform distribution of RD's per degree of β, the discontinuity cone angle, yields lower limit estimates for these ratios of 0.89, 0.66, and 0.43, for the respective locations, but the proportional change with r is similar to the upper limit

estimate.

5. The distributions of the longitudes of the TD normals (ϕ_N) tend to have peaks approximately perpendicular to the average field for the "full" sets, as expected, but are broad. The longitude distributions for "clean" RD's are also broad with peaks near an average of the radial and long-term average field longitude directions for the 0.46 and 0.72 AU positions. Also the peak for these two distributions tends to shift clockwise for increasing r. (Figure 8).

6. The distributions of the latitudes of the normals (θ_N) are approximately symmetric about the solar equatorial plane and usually symmetric about the long-term field latitude direction for both TD's and RD's. The TD distributions, however, show a tendency to possess either a high or low inclination, especially for the "full" sets. (Figure 9).

7. The discontinuity angle (ω) distributions are independent of r for a given type, giving $\langle\omega\rangle \approx 90^\circ$ for RD's and $\langle\omega\rangle = 80^\circ$ for TD's. Even though these distributions are broad this difference in $\langle\omega\rangle$ by type is significant. There is a near absence of TD's with $150^\circ \leq \omega \leq 160^\circ$ (Figure 10).

8. The average DD thickness $\langle\tau\rangle$ increases markedly with increasing r: $\sim$1200, $\sim$1600, and $\sim$2700 km at 0.46, 0.72, and 1.0 AU, respectively, independent of type, and the distributions of τ are broad at all locations. The TD distributions are slightly narrower than the RD distributions when those cases where $\tau > 56{,}000$ km are ignored. (Figure 11).

9. When the DD thicknesses are normalized with respect to the local proton gyroradius (τ_L) for each event separately, the average thickness for all r and both types is nearly constant at 43 ± 6 proton gyroradii. (See Tables 1, 2 and 3, row 4).

10. No obvious general relationship exists between τ and ω (Figure 12).

Allowing for the ambiguities and variabilities mentioned in the Introduction and discussion of figures (e.g., occasional uncertainty of type and time variability of DD sample), we will assume that this summary of observations reasonably represents average characteristics for the region $0.46 \leq r \leq 1.0$ AU, independent of longitude about the sun, during the time of the Mariner 10 observations (Dec. 1973-April 1974).

It is of great interest to compare the Mariner 10 DD results with those of studies based on data from other spacecraft. Of particular interest is an intercomparison between Mariner 10 and Helios results, since the Mariner 10 heliocentric distance range was included within the Helios 1 and 2 ranges, which extended from 1 AU to 0.31 and 0.29 AU, respectively. As will be shown in the following discussion, there is considerable general agreement but also points of disagreement between the two sets of results. The differences are not completely understood, although undoubtedly some of them are attributable to (a) different event selection techniques (manual selection for Mariner 10, machine selection for Helios), (b) different numbers of events in the statistics (a total of 644 DD's in the Mariner 10 set, and 1427, in some cases even more, in the Helios set); (c) different time periods of data coverage (Helios 1 launched Dec. 10, 1974 and Helios 2, Jan. 15, 1976 compared with the Dec. 19, 1973 - April 1974 period for the Mariner 10 study); (d) different latitude coverage as a function of solar longitude, which can make a difference since there is a dependence of the occurrence (and possibly other properties) of DD's on V_{SW} (Barnstorf, 1980); and V_{SW} varies not only with longitude but also can vary markedly with latitude; and (e) closer approach to the sun by the Helios spacecraft than the 0.46 AU perihelion of Mariner 10. Most of these points apply to comparisons with data from other spacecraft as well as with those from Helios.

Concerning point (a), we shall not discuss our selection procedure further here, except to emphasize that we believe it gives better quality control on events selected (i.e., it provides certainty with regard to the

detailed appearance of the events) at the sacrifice of number of events (i.e., some events must unquestionably be overlooked), as implied in point (b). Although no constraints were placed on the rate of change of the field for the Mariner 10 study, none of the events we selected violated the tightest rate-limiting constraint generally used in automatic selection; i.e., one degree per second was the slowest rate allowed.

The first item in our results summary on the decreasing DD occurrence rate with increasing heliocentric distance (r) implies either that DD's are generated closer to the sun than 0.46 AU and appear to decrease in number with increasing r due to their spatial distribution as they travel outward or that the ratio of generation rate to disappearance rate becomes smaller as r increases. It is conceivable that both possibilities are operative. Between 1 and 8.5 AU, Pioneers 10 and 11 also found a decreasing rate of occurrence with increasing distance (Tsurutani and Smith, 1979). Large variations from day to day and even from solar rotation to solar rotation were found, but the results implied on average 25% per AU radial gradient. Mariner 10 found a decrease of 66% from 0.46 to 1.0 AU. As indicated earlier, for this part of the study, Mariner 10 also used an automatic selection procedure. Extending the best fit power law (Figure 1) predicts a percent rate of decrease which reduces for each 1 AU range, with a decrease of ~14% being predicted for the range 8 to 9 AU. The average for the 8 1-AU intervals between 1 and 9 AU is found to be 28%, not very different from the average 25% gradient derived from the Pioneer observations.

Also Helios 1 and 2 found a decrease in average occurrence rate with increasing distance (Barnstorf, 1980), but with somewhat smaller overall variation than seen by Mariner 10. Note that the Helios data were corrected for azimuthal spacecraft speed relative to the rotational speed of the sun. This correction increases the count rates, most markedly near the sun. Helios 1 found a decrease from 2.4 to 1.4 DD's/hour between ~0.3 and 1 AU, and for Helios 2 the rate decreased from 2.6 to 1.2. This gives percent rates of decrease of 42% and 54%, respectively, over the ranges of observation. Thus it appears that a decrease in occurrence with distance has been observed by all deep space probes with which DD's have been

studied, although the rate varies with time and radial distance.

Tsurutani and Smith (1979) concluded that the decrease in rate found by Pioneer 10 could have been a selection effect related to the observed increase in thickness with distance. That is not as likely to have been the case for Helios or Mariner 10, since generally thinner structures are observed inward from 1 AU, and thus they usually would not exceed a fixed maximum thickness selection criterion appropriate for 1 AU. The physical implications of an occurrence rate decrease with greater distance from the sun will be discussed in the concluding remarks.

The second item in our results summary (λ_2/λ_3 independent of r) indicates that the degree to which one may define a discontinuity plane for a DD is on average independent of r. This has not yet been studied separately for TD's and RD's.

The Helios results offer the only possibility for direct comparison of relative normal component distributions (summary items 3 and 4). In order to compare the Mariner 10 DD's by percentage of type (i.e., TD's vs. RD's) with the results of Helios (Barnstorf, 1980), we now split up the distribution of $B_n/\langle B\rangle$ by leaving out an "uncertainty band" over the domain $0.3 \leq B_n/\langle B\rangle \leq 0.7$, as was done in the Helios study. Then considering the number of cases for which $B_n/\langle B\rangle < 0.3$ (which we generally classify as TD's and which constitute the primary peak in the distribution), we find that there is a combined total fraction (for all r) for Mariner 10 of 49%, or separately 56%, 55%, and 44% for r = 1.0, 0.72 and 0.46 AU, respectively. These values are to be compared with 40% for Helios (for all r). Similarly, comparing the fractions with $B_n/\langle B\rangle > 0.7$, we have 24% for the Mariner 10 total, and 18%, 23% and 28% separately at 1.0, 0.72 and 0.46 AU, compared with a 32% total for Helios. This gives the ratios (% < 0.3)/% > 0.7) = 1.25 for Helios compared with 2.04 for the Mariner 10 total data and 3.11, 2.39, and 1.57 for the three Mariner 10 locations separately. Thus, at all distances Mariner 10 found relatively fewer cases of large relative normal DD's that could be interpreted with certainty as RD's. Further, Mariner 10 saw a 57% increase in $B_n/\langle B\rangle > 0.7$ cases between 1 AU and 0.46 AU (relative to 1 AU), and a 21% decrease in $B_n/\langle B\rangle < 0.3$, consistent with

our previous conclusion that the ratio no. TD's/no. RD's increased for increasing r.

The ratios given above are to be compared with the TD/RD ratios determined simply on the basis of using $B_n/\langle B\rangle = 0.3$ as a partition boundary (item 3 in our summary) or with σ_F/F vs β used as a discriminator (item 4), which gives slightly higher values that range from 1.5 to 0.86 for r = 1.0 to 0.46 AU. The result in item 3 is indirect evidence that the relative number of TD's to RD's decreases as r decreases. If, indeed, the DD's are generated primarily near the sun, this observation implies that RD's disappear more easily than TD's on average. Item 4 confirms this supposition, where a more strict discrimination was used in determining type. Although different criteria were used for Helios, a refined ratio of the number of TD's to the number of RD's = 2.0 was determined for those observations (for all N), where again TD's were defined for $B_n/\langle B\rangle < 0.3$. For RD's it was required that $B_n/\langle B\rangle > 0.5$ must hold and, in addition, two angles α and β (which are functions of $\Delta\vec{V}$, $\Delta\vec{B}$, $\Delta\rho$) had to fall within certain ranges; specifically: $30^\circ<\alpha<60^\circ$, $0^\circ<\beta<30^\circ$, and $150^\circ<\beta<180^\circ$, where $\alpha = \tan^{-1}(\sqrt{4\pi/\rho}\,|\vec{v}|/|\vec{b}|)$, $\beta = \cos^{-1}(P(\vec{v}\cdot\vec{b})/|\vec{r}\cdot\vec{b}|)$, $\vec{v} = \vec{V}_1 - \vec{V}_2$, and $\vec{b} = \vec{B}_1/\rho_1 - \vec{B}_2/\rho_2$, where the subscripts 1 and 2 denote the two sides of a DD.

In DD survey studies at 1 AU using Explorer 43 measurements, Burlaga et al. (1977) determined no. TD's/no. RD's = 2.8, assuming that $B_N < 2$ nT identifies TD's and $B_N > 3$ nT signifies RD's at 1 AU. For $\omega \geq 30^\circ$, there were 122 of the former and 43 of the latter, for a total of 165 DD's. Those authors felt that their determination was not unambiguous, however, since cases with small ω ($< 30^\circ$) were excluded from the study. As indicated earlier, such an exclusion is a practical necessity, since for $\omega < 30^\circ$ the errors in estimated normals become unacceptable large. In a previous study, Burlaga (1971) concluded that < 25% of his cases could be RD's. Belcher and Solodyna (1975) concluded that > 75% of their cases were RD's. Subsequently, Solodyna et al. (1977) have found that TD's dominate in low velocity solar wind and RD's dominate in high velocity wind. This is consistent with there being (relatively) fewer RD's in the Mariner 10 data set than in the Helios set, since the three Mariner 10 intervals were selected to correspond to predominately moderate speed solar wind, whereas

the Helio observations were taken during both low and high speed solar wind periods.

The next DD property which we studied was the orientation of the DD normals (items 5 and 6 in the summary) expressed in terms of longitude angle, ϕ_N, and latitude angle, θ_N. The Mariner 10 ϕ_N distributions show that TD normals are most likely to be oriented perpendicular to the long-term mean magnetic field. (On a short time scale this must be true ideally for a TD.) This result is in agreement with both Helios (Barnstorf, 1980) and 1 AU observations (Burlaga et al., 1977). The Mariner 10 distributions show that there is also a tendency for the normals in some cases to be nearly parallel to the long-term mean field, viz., the secondary peak in the ϕ_N distributions. The RD ϕ_N's were found to be more broadly distributed in all cases i.e., more nearly isotropically distributed near 1 AU (Mariner 10 and 1 AU results of Burlaga et al., 1977), but with a tendency to become more peaked along the mean field direction nearer the sun (Mariner 10 and Helios). It is possible that the smaller secondary peak near the mean field direction, in the Mariner 10 "TD" distributions is partially due to contamination of the TD's by some fraction of small-normal RD's.

As stated earlier, there is nothing particularly noteworthy about the θ_N distributions. They indicate that the normals tended to lie on average nearer to the solar equatorial plane than perpendicular to it (with the exception of the 1 AU TD's, where the most probable value was $\sim 50^\circ$). The RD's show again a tendency toward a more isotropic distribution than the TD's. In these characteristics there is general agreement with the 1 AU results of Burlaga et al. (1977) and the Helios results (Barnstorf, 1980). The Helios measurements, however, gave a θ_N distribution for RD's with most probable $\theta_N \approx 0^\circ$ and with a symmetry about 0° not found in the other observations.

Our study of the discontinuity angle ω (summary item 7) shows that ω is independent of r for both RD's and TD's. The Helios results have confirmed that conclusion. The latter results have suggested, however, that there is a dependence on the macrostructure of the IMF. There is a

relatively wide range of values for $\langle\omega\rangle$ among the results of the various DD studies, with the highest average values being those from Mariner 10. A comparison of the respective distributions suggests that for Mariner 10 there were relatively fewer cases with $30^{\circ} \leq \omega \leq 40^{\circ}$. A large fraction of the candidate DD's with ω in that range were found to have $\lambda_2/\lambda_3 < 2$, which disqualified them from consideration, as was the case for almost all candidates with $\omega < 30^{\circ}$. Also, in some of the other DD investigations the angle studied was actually the angle of rotation of the total field across the DD, which is identically equal to ω for ideal TD's but less than ω for RD's. This would contribute to a smaller average value than would be determined for ω.

The final DD property of interest was the thickness, both in km (τ) and ion larmor radii (τ_L), and its variation with r. The Mariner 10 thicknesses in km (summary item 8) are generally consistent with the Helios TD results. However, where Mariner 10 found the RD thicknesses to be comparable to those of the TD's, Helios found RD's to have almost double the average thickness of the TD's. In terms of gyroradii (summary item 9), a value of $\tau_L = 43 \pm 6\ R_L$ is estimated for both types of DD's and all r for Mariner 10, compared with 47 R_L for Helios for a similar composite data set. Some of the difference in results for τ may be due to the assumption of a constant $V_{SW} = 400$ km/s in the Mariner 10 analysis, but perhaps more likely it is due to the differences in selection procedures. As indicated earlier, there was no discrimination against broad structures in the Mariner 10 DD selection. It is of interest to note that these current sheets are thinner (in km) by an order of magnitude or more than the heliographic current sheet observed by Helios 1 on "sector boundary" crossings (Behannon et al., 1980).

What can be concluded from these results? The Mariner 10 observations have confirmed that the solar wind is interlaced throughout with current sheets both in the form of static structures and discrete waves (RD's). (The latter are found to be present in significant numbers.) These discontinuities are important as scatterers of cosmic rays and they are known to influence geomagnetic activity. The decrease in occurrence rate with increasing heliocentric distance first observed by Mariner 10

(Behannon, 1976) has been confirmed by the Helios 1 and 2 spacecraft and probably also by Pioneer 10 and 11. This result suggests that either the DD's are unstable or there exists a geometric effect in the spatial distribution of DD's that produces the observed gradient. The fact that DD thickness in km is found to increase as r increases but remains approximately constant in units of gyroradii implies that the current sheets are quasistationary, with the structure determined by the proton drift current $\vec{J}$. That this appears to be true for both TD's and RD's suggests that RD's may not be simply the smoothly continuous tail of the Alfvén wave distribution, but may be distinct entities. The result that ω is independent of r is also consistent with stability, or, if there is an instability operative, it is not the Kelvin-Helmholtz instability.

One is led to conclude that the most likely explanation for the dependence of occurrence rate on r is a geometric one and is related to the expansion of the solar wind. Whether these current sheets are discrete, spatially-limited entities like "leaves in the wind", are spherical shells or shell segments, or are filamentary ribbons connecting back to the sun (or possibly have a still different configuration) has not yet been clearly established. Additional multispacecraft studies may permit a resolution of such remaining questions as the spatial extent and shape of DD's in the IMF and their stability in time.

Acknowledgments

We are grateful to L. F. Burlaga for reading the manuscript and we thank him and F.M. Neubauer for helpful comments on the interpretation. We also thank N. F. Ness, the principal investigator of the Mariner 10 magnetic field experiment, for his general support and comments, and D. Howell and P. Harrison for the Mariner 10 data processing effort.

References

Barnstorf, H., Stromschichten in interplanetaren Plasma, Ph.D. Thesis, Institut fuer Geophysik und Meteorologie, Technische Universitaet Braunschweig, Federal Republic of Germany, 1980.

Behannon, K. W., Observations of the interplanetary magnetic field between 0.46 and 1 AU by the Mariner 10 spacecraft, Ph.D. Thesis, Catholic University 1975; NASA/GSFC X-document 692-76-2, January 1976.

Behannon, K.W., and L.F. Burlaga, Alfvén waves and Alfvénic fluctuations in the solar wind, contributions to the Fourth Solar Wind Conference, August 28-September 1, 1978, Burghausen, Federal Republic of Germany, NASA/GSFC TM 79711, 1978; to be published in conference Proceedings, Ed. H.R. Rosenbauer, Springer-Verlag, 1980.

Behannon, K.W., F.M. Neubauer, and H. Barnstorf, Fine-scale characteristics of interplanetary sector boundaries, submitted to J. Geophys Res., 1980.

Belcher, John W., Statistical properties of interplanetary microscale fluctuations, J. Geophys. Res., 80, 4713, 1975.

Belcher, J.W., and L. Davis, Jr., Large-amplitude Alfvén waves in the interplanetary medium, 2, J. Geophys Res., 76, 3534, 1971.

Belcher, J. W., and C. V. Solodyna, Alfvén waves and directional discontinuities in the interplanetary medium, J. Geophys. Res., 80, 181, 1975.

Burlaga, L. F., Directional discontinuities in the interplanetary magnetic field, Solar Phys., 7, 54, 1969a.

Burlaga, L.F., Large velocity discontinuities in the solar wind, Solar Phys., 7, 72, 1969b.

Burlaga, L. F., On the nature and origin of directional discontinuities, J. Geophys. Res., 76, 4360, 1971.

Burlaga, L. F., J. F. Lemaire, and J. M. Turner, Interplanetary current sheets at 1 A.U., J. Geophys. Res., 82, 3191, 1977.

Denskat, K.U., and L.F. Burlaga, Multispacecraft observations of microscale fluctuations in the solar wind, J. Geophys. Res., 82, 2693, 1977.

Fitzenreiter, R.J., Two-spacecraft measurements of the structure of tangential discontinuities, EOS, Transactions A.G.U., 60, 365 (SS23 abstract), 1979.

Hartle, R.E. and A. Barnes, Non-thermal heating in the two-fluid solar wind model, J. Geophys. Res., 75, 6915, 1970.

Lepping, R. P. and K. W. Behannon, Magnetic field directional discontinuities: 1. Minimum variance errors, J. Geophys. Res. 85, 4695, 1980.

Lepping, R. P., K. W. Behannon, and D. R. Howell, A method of estimating zero level offsets for a dual magnetometer with flipper on a slowly rolling spacecraft: Application to Mariner 10, NASA/GSFC X-692-75-268, October 1975.

Martin, R. N., J. W. Belcher, and A. J. Lazarus, Observations and analysis of abrupt changes in the interplanetary plasma velocity and magnetic field, J. Geophys. Res., 78, 3653, 1973.

Ness, N.R., K.W. Behannon, R.P. Lepping, Y.C. Whang, and K.H. Schatten, Magnetic field observations near Venus: Preliminary results from Mariner 10, Science, 183, 1301, 1974.

Ness, N.F., A.J. Hundhausen, and S.J. Bame, Observations of the interplanetary medium, Vela 3 and IMP 3, 1965-1967, J. Geophys. Res., 76, 6643, 1071.

Ness, N. F., C. S. Scearce, J. B. Seek and J. M. Wilcox, Summary of results from the IMP-1 magnetic field experiment, Space Res., 6, 581, 1966.

Neubauer, F. M. and H. Barnstorf, Recent observational and theoretical results on discontinuities in the solar wind, Fourth Solar Wind Conference, August 28 - September 1, 1978, Burghausen, Federal Republic of Germany; to be published in Conference Proceedings, ed. H.R. Rosenbauer, Springer-Verlag, 1980.

Sari, James W., Modulation of low energy cosmic rays, Ph.D. Thesis, University of Maryland, 1972, NASA/GSFC X-692-72-309, August 1972.

Scudder, J.D., and S. Olbert, A theory of local and global processes which affect solar wind electrons. 2. Experimental support, J. Geophys. Res., 84, 6603, 1979.

Seek, J. B., J. L. Scheifele, and N. F. Ness, GSFC magnetic field experiment: Mariner 10, NASA/GSFC X-695-77-256, October 1977.

Sen, A.K., Stability of hydromagnetic Kelvin-Helmholtz discontinuity, Phys. Fluids, 6, 1154, 1963.

Siscoe, G. L., L. Davis, Jr., P. J. Coleman, Jr., E. J. Smith and D. C. Jones, Power spectra and discontinuities of the interplanetary magnetic field: Mariner 4, J. Geophys. Res., 73, 61, 1968.

Smith, E. J., Identification of interplanetary tangential and rotational discontinuities, J. Geophys. Res., 78, 2054, 1973a.

Smith, E. J., Observed properties of interplanetary rotational discontinuities, J. Geophys. Res., 78, 2068, 1973b.

Solodyna, C. V., J. W. Sari, and J. W. Belcher, Plasma field characteristics of directional discontinuities in the interplanetary medium, J. Geophys. Res., 82, 10, 1977.

Sonnerup, B.U.O., and L. J. Cahill, Magnetopause structure and attitude from Explorer 12 observations, J. Geophys. Res., 72, 171, 1967.

Tsurutani, B. T., and E. J. Smith, Interplanetary discontinuities: Temporal variations and the radial gradient from 1 to 8.5 AU, J. Geophys. Res., 84, 2773, 1979.

Whang, and C.C. Chang, An inviscid model of the solar wind, J. Geophys. Res., 70, 4175, 1965.

TABLE 1

STATISTICAL CHARACTERISTICS OF DD'S

(Distance = 1.00 A.U.)

	Clean R.D.'s (N=62)		Clean T.D.'s (N=29)		Full Mixed ["T.D.'s"] (N=91)		"Bad" (N=10)	
Parameter	AVE	RMS	AVE	RMS	AVE	RMS	AVE	RMS
ω	90.4°	38.5°	85.7°	33.6°	79.0°	32.2°	71.9°	28.1°
β	46.6°	17.8°	82.3°	4.9°	81.6°	4.9°	55.9°	13.4°
τ(km)	2670	2460	3500	2720	2640	2130	2270	1600
$\tau_L(L_R)$	49.6	53.6	54.2	56.1	43.6	44.4	30.8	25.9
ϕ_N	188.2°	54.5°	193.1°	41.6°	194.8°	39.4°	203.5°	41.5°
θ_N	0.6°	33.1°	9.4°	33.8°	3.2°	36.2°	9.9°	29.7°
F(nT)	5.6	2.1	5.0	2.0	5.2	2.0	4.2	0.80
$\lvert B_n \rvert$(nT)	3.9	2.3	0.69	0.47	0.79	0.56	2.3	0.96
σ_B (nT)	0.21	0.14	0.21	0.11	0.17	0.10	0.20	0.11
λ_2/λ_3	4.9	4.3	6.5	9.9	6.8	9.6	4.2	3.9

TABLE 2

STATISTICAL CHARACTERISTICS OF DD'S

(Distance = 0.72 A.U)

	Clean R.D.'s (N=88)		Clean T.D.'s (N=37)		Full Mixed ["T.D.'s"] (N=103)		"Bad" (N=15)	
Parameter	AVE	RMS	AVE	RMS	AVE	RMS	AVE	RMS
ω	87.4°	39.8°	99.7°	25.1°	80.8°	29.2°	90.5°	42.9°
β	45.4°	16.6°	83.4°	4.8°	83.3°	4.9°	54.6°	14.6°
τ (km)	1460	1330	1860	2240	1720	2010	2220	2170
$\tau_L(L_R)$	37.7	35.5	41.4	56.0	40.3	49.2	45.6	38.8
ϕ_N	178.5°	51.3°	198.9°	43.3°	202.7°	38.5°	192.6°	38.8°
θ_N	0.0°	29.6°	8.3°	31.3°	6.9°	34.3°	-0.1°	32.3°
F(nT)	10.9	3.2	8.9	2.8	9.8	3.2	9.4	2.8
$\lvert B_n \rvert$(nT)	7.3	2.9	1.1	0.69	1.1	0.82	5.2	2.3
σ_B(nT)	0.32	0.25	0.41	0.25	0.34	0.24	0.52	0.38
λ_2/λ_3	6.0	6.5	12.0	10.1	11.1	14.5	7.5	12.0

TABLE 3

STATISTICAL CHARACTERISTIC OF DD's

(Distance = 0.46 A.U.)

	Clean R.D.'s (N=139)		Clean T.D.'s (N=31)		Full Mixed ["T.D.'s"] (N=120)		"Bad" (N=16)	
Parameter	AVE	RMS	AVE	RMS	AVE	RMS	AVE	RMS
ω	91.3°	38.3°	103.9°	36.6°	80.0°	33.3°	112.3°	39.5°
β	44.7°	18.7°	81.9°	4.9°	82.5°	4.9°	60.5°	10.1°
τ(km)	1300	1400	1750	2060	1170	1500	1790	2170
$\tau_L(L_R)$	48.2	48.9	46.4	55.5	38.0	44.8	72.7	104.0
ϕ_N	176.7°	46.0°	174.5°	42.8°	175.1°	50.0°	173.3°	59.9°
θ_N	3.8°	33.0°	9.2°	31.4°	6.8°	37.2°	8.4°	38.9°
F(nT)	18.3	3.3	14.4	5.7	16.9	4.3	17.2	6.2
$\lvert B_n \rvert$(nT)	12.4	4.7	2.1	1.4	2.3	1.5	8.3	3.7
σ_B(nT)	0.53	0.40	0.73	0.55	0.55	0.42	1.2	0.66
λ_2/λ_3	6.6	7.1	10.8	8.1	13.4	15.3	5.9	4.8

FIGURE CAPTIONS

Figure 1. Occurrence rate dependence of magnetic field directional discontinuities on heliocentric radial distance. The large scale field sector polarity is shown: positive sign represents "toward" the sun and negative sign away. θ_{SEQ} is the latitude of the spacecraft with respect to the solar equatorial plane.

Figure 2. Mariner 10 high resolution (40 ms) data during the traversal of two interplanetary DD's, illustrating that such structures can have differing time scales but not differ appreciably in magnetic field variation. At the left is shown a 2 minute interval of data and at the right a 20 s interval. In both cases is given (from top to bottom) the solar ecliptic (SE) direction angles ϕ, θ, the field magnitude B, and the SE cartesian coordinates of the field B_x, B_y, B_z. The vertical dashed lines superimposed on the coordinate data represent the precise beginning and end of the DD transition zone, and the horizontal solid lines represent the quasisteady state of the field immediately before and after the transition zone.

Figure 3. The intermediate to minimum eigenvalue ratio shown as a percent distribution for ω's exceeding 30° and for data taken at three distances from the sun (see text). N denotes the number of DD's at each location.

Figure 4. Distributions of $|B_n|/B$ for $\lambda_2/\lambda_3 \geq 2.0$. The angle β is the discontinuity cone angle, $\beta = \cos^{-1}(|B_n|/B)$. The vertical dashed lines indicate the separation point between "TD's" (on the left) and RD's (on the right).

Figure 5. Scatter diagram of discontinuity data at 1.0 AU showing relative magnitude rms deviation σ_F/F (from measurements across the DD zone) as a function of β (see text). The arrows and numbers at the top-right, just outside the box, represent in all cases but one (.260) legitimate TD's whose σ_F/F was too large to plot.

Figure 6. Similar to Figure 5, except it holds for R = 0.72 AU.

Figure 7. Similar to Figure 5, except it holds for R = 0.46 AU.

Figure 8. Distributions of the longitudes (ϕ_N) of the discontinuity normals with respect to location and type. Also for completeness "clean" versus full sets are represented along with the overall average field direction ($\phi_{\langle \vec{B} \rangle}$) for each set (see text).

Figure 9. Distributions of the latitudes (θ_N) of the discontinuity normals with respect to location and type (see related Figure 8).

Figure 10. Distributions of the discontinuity angle ω given separately for location and type. Mean values given in each case have only a relative value since most cases with $\omega < 30^\circ$ were excluded from the study (see text).

Figure 11. Discontinuity thickness distributions (in units of 100 km) with respect to location and type. The statements in parentheses represent the percentage of those DD's whose thicknesses are greater than 5600 km.

Figure 12. Distributions of DD thickness τ averaged over 20° intervals of the discontinuity angle ω. Results are shown separated for RD's (left) and TD's (right). Vertical bars give $\pm \sigma/\sqrt{N}$ for each average, indicating variability within the data averaged (see text). No obvious general relationship between τ and ω is observed.

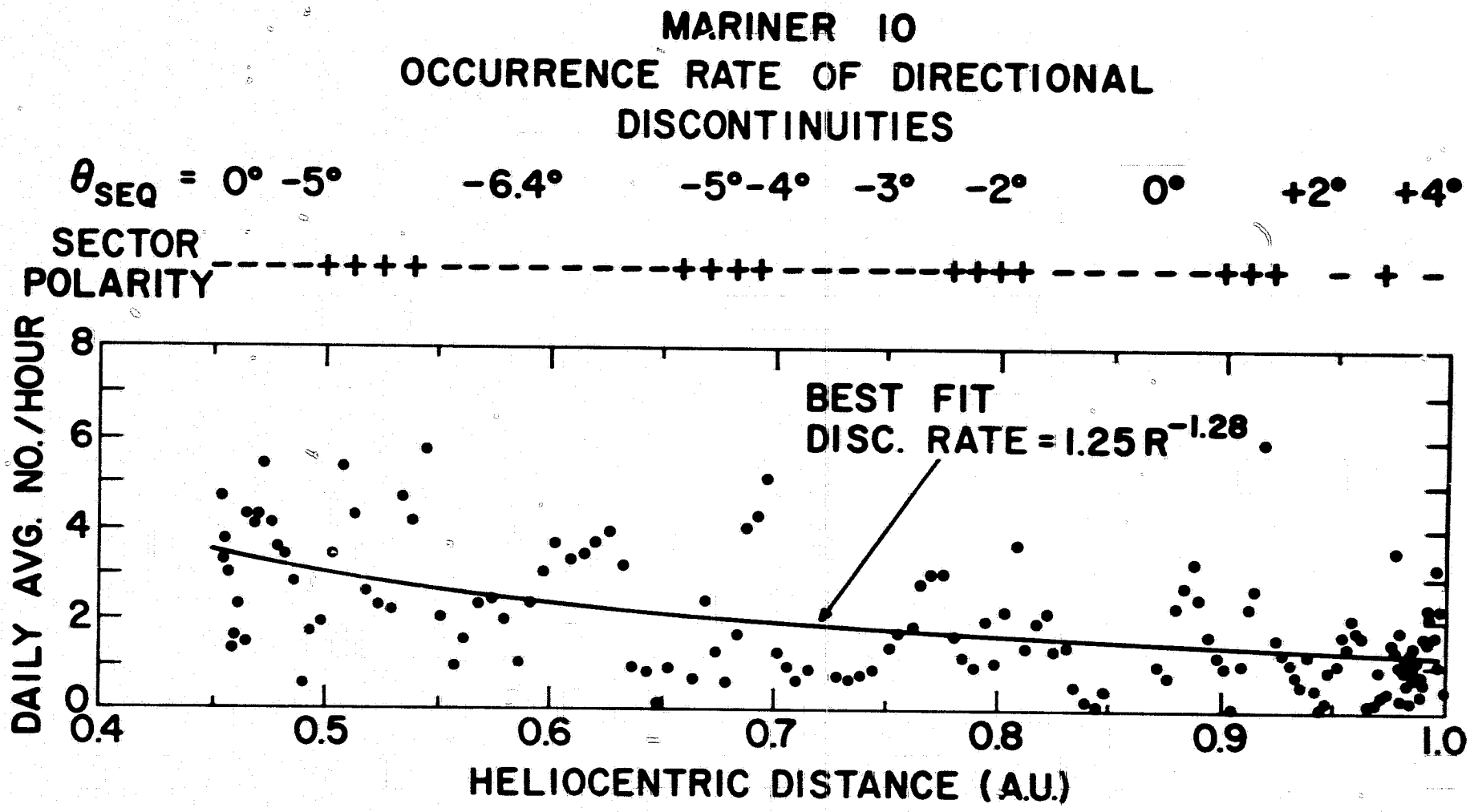
MARINER 10
OCCURRENCE RATE OF DIRECTIONAL DISCONTINUITIES
θSEQ = 0° -5° -6.4° -5°-4° -3° -2° 0° +2° +4°
SECTOR POLARITY
BEST FIT
DISC. RATE = 1.25 R^-1.28
DAILY AVG. NO./HOUR
HELIOCENTRIC DISTANCE (A.U.)
0
2
4
6
8
0.4
0.5
0.6
0.7
0.8
0.9
1.0

Figure 1

MARINER 10

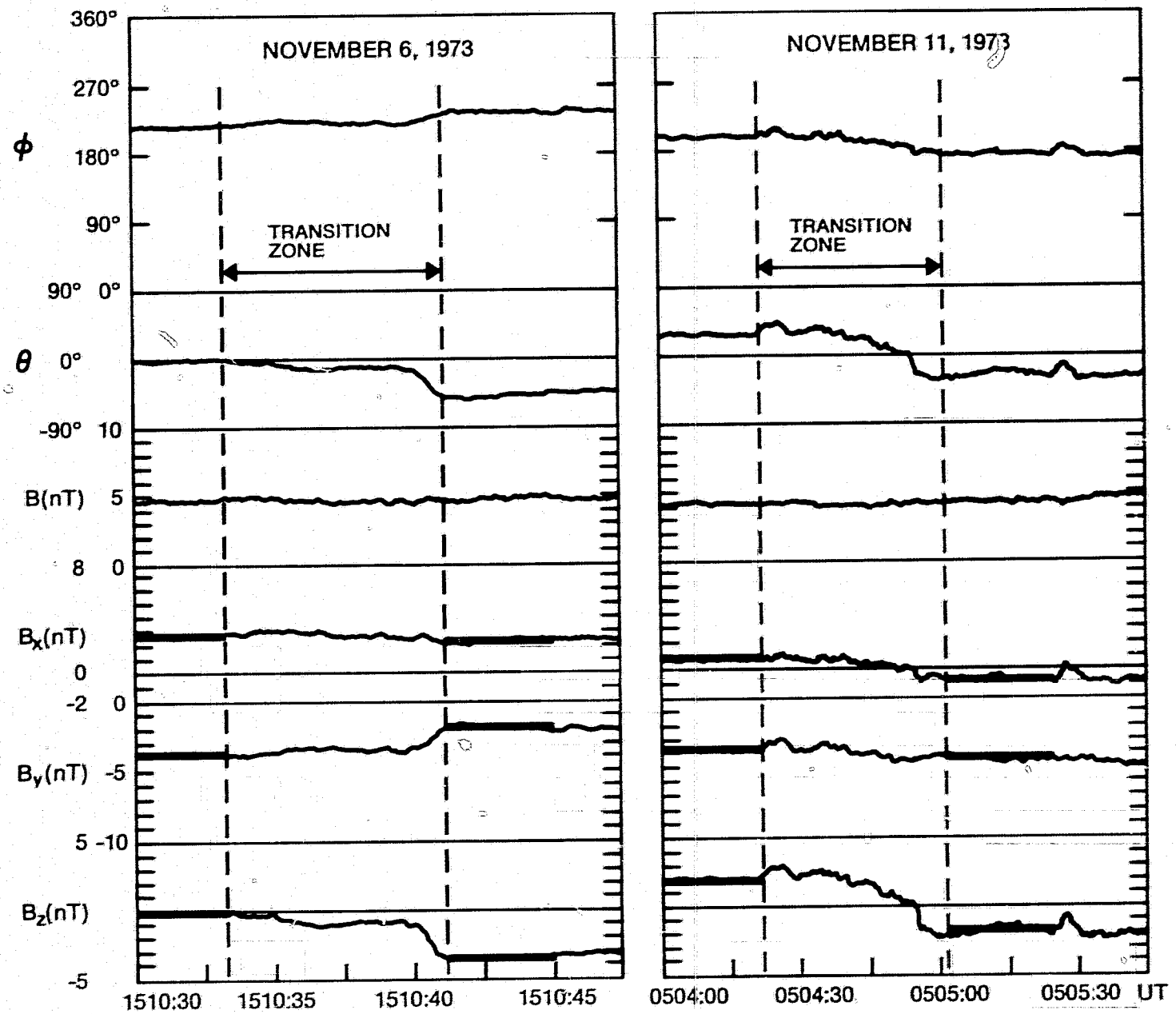

Figure 2

λ_2/λ_3 DISTRIBUTIONS FOR $\omega \geq 30°$ AND $\lambda_2/\lambda_3 \geq 2.0$

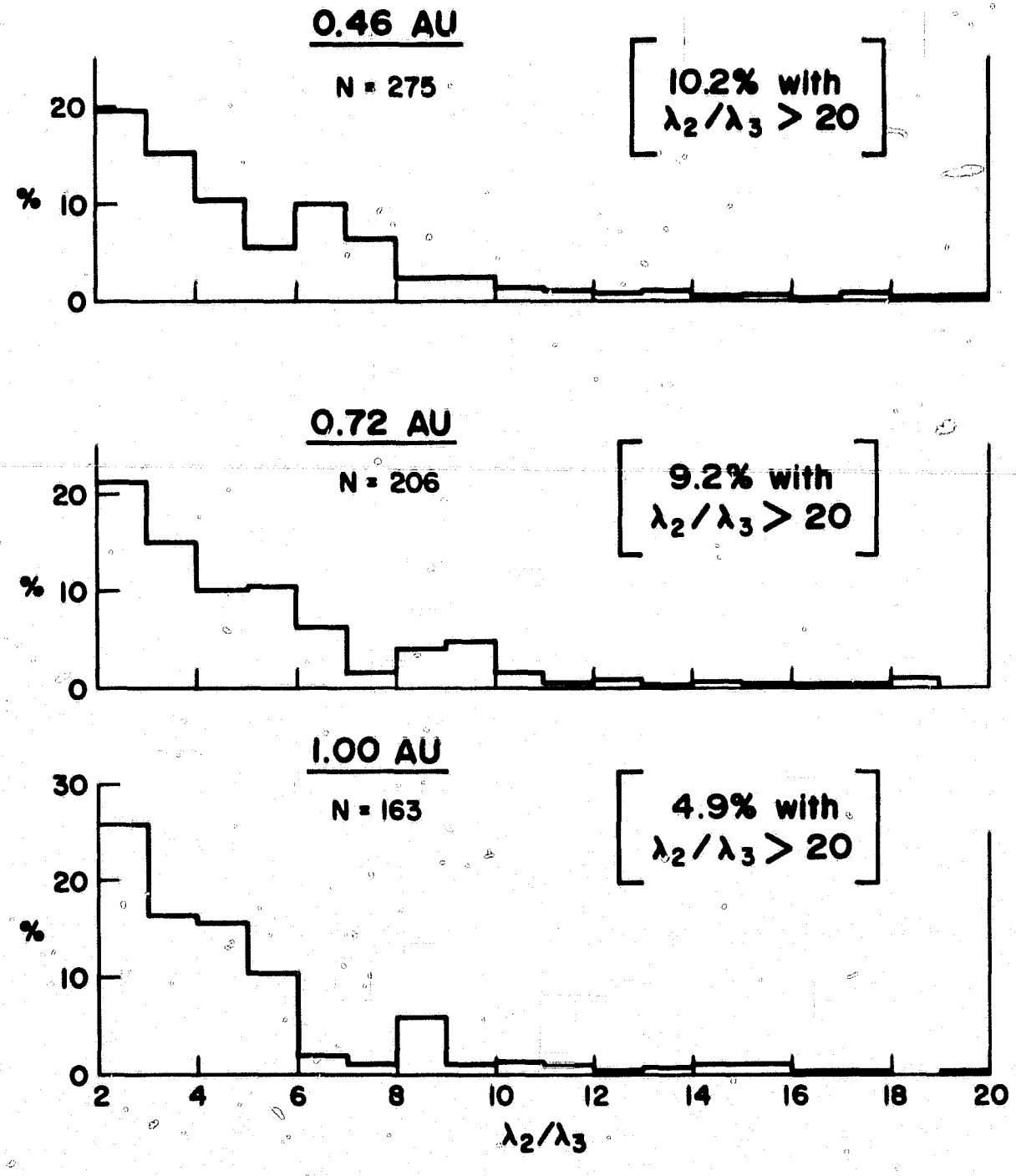

Figure 3

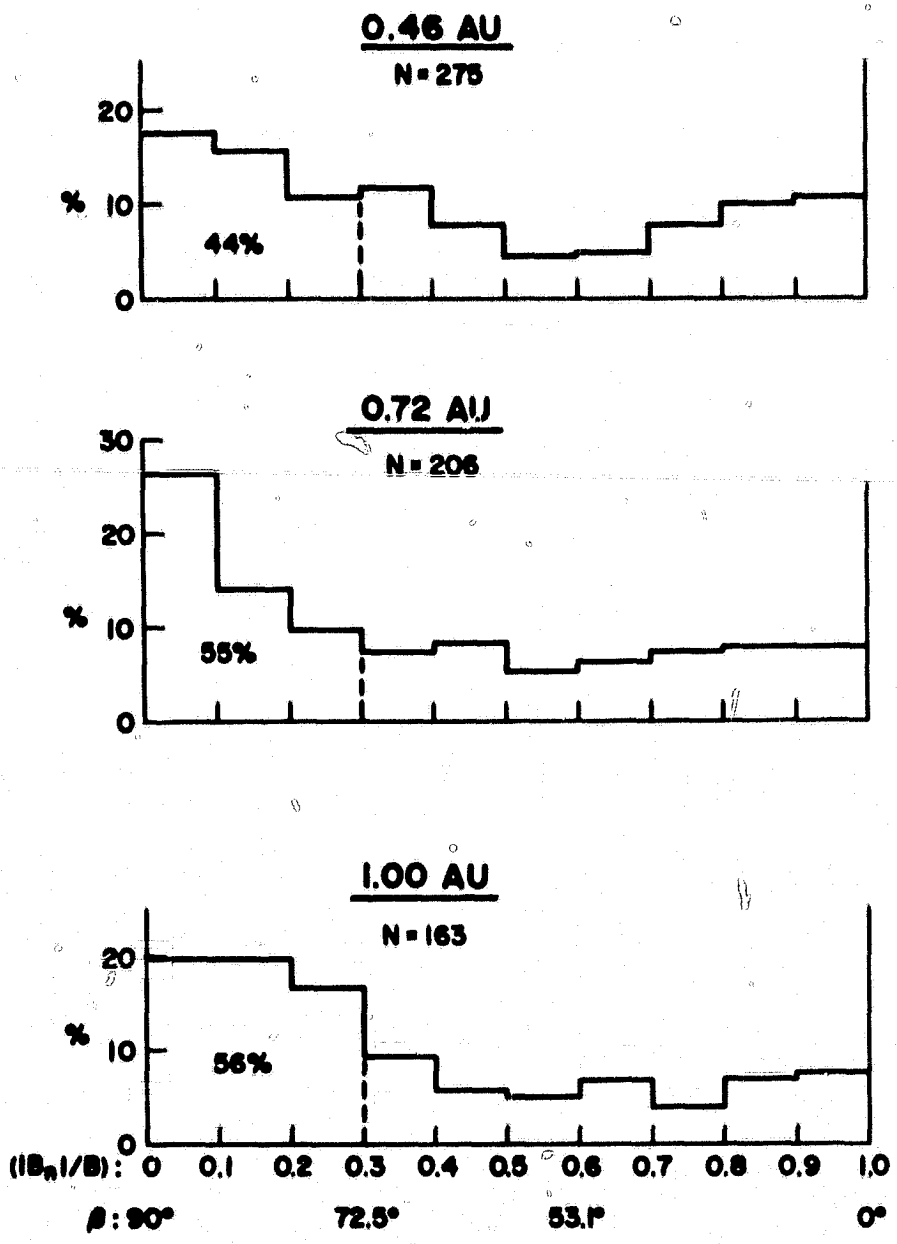
RELATIVE NORMAL COMPONENT DISTRIBUTIONS FOR $\lambda_2/\lambda_3 \geq 2.0$
0.46 AU
N = 275
20
%
10
0
44%
0.72 AU
N = 206
30
20
%
10
0
55%
1.00 AU
N = 163
20
%
10
0
56%
(|B_n|/B): 0 0.1 0.2 0.3 0.4 0.5 0.6 0.7 0.8 0.9 1.0
β: 90° 72.5° 53.1° 0°

Figure 4

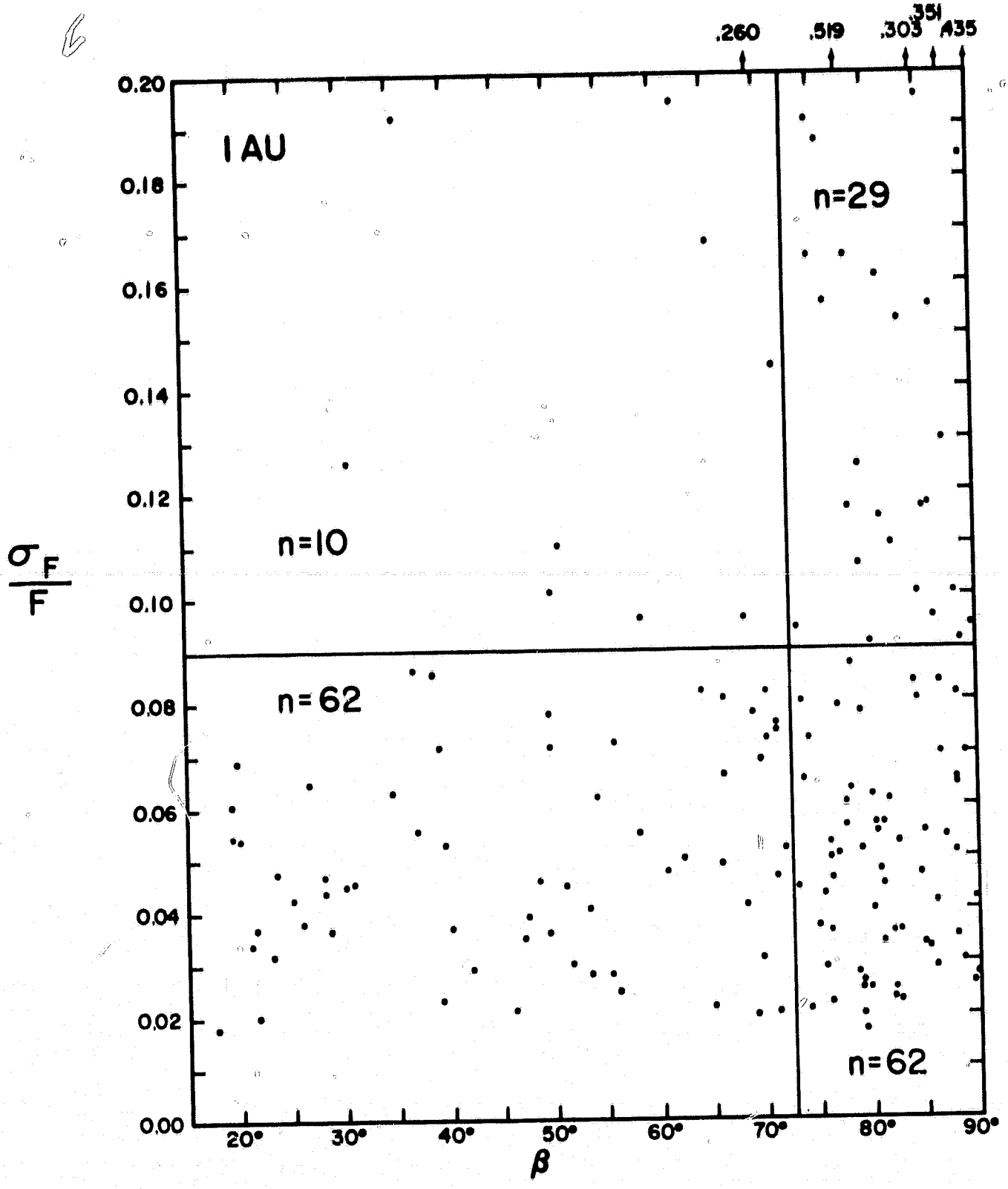
.260
.519
.303
.351
.435
1 AU
n=29
n=10
n=62
n=62
0.20
0.18
0.16
0.14
0.12
0.10
0.08
0.06
0.04
0.02
0.00
20°
30°
40°
50°
60°
70°
80°
90°
β
σF/F

Figure 5

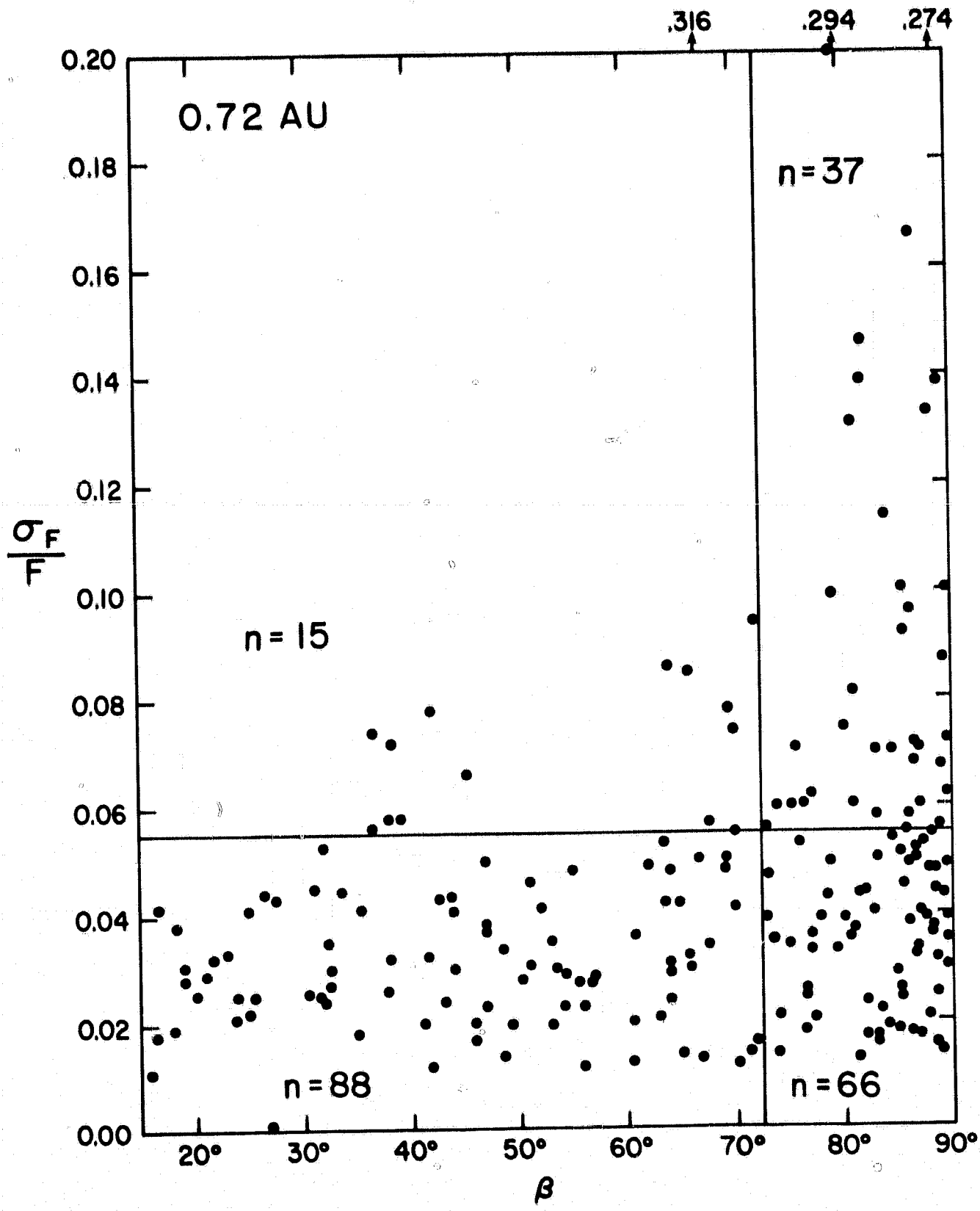
.316
.294
.274
0.72 AU
n = 37
n = 15
n = 88
n = 66
0.20
0.18
0.16
0.14
0.12
0.10
0.08
0.06
0.04
0.02
0.00
σF/F
20°
30°
40°
50°
60°
70°
80°
90°
β

Figure 6

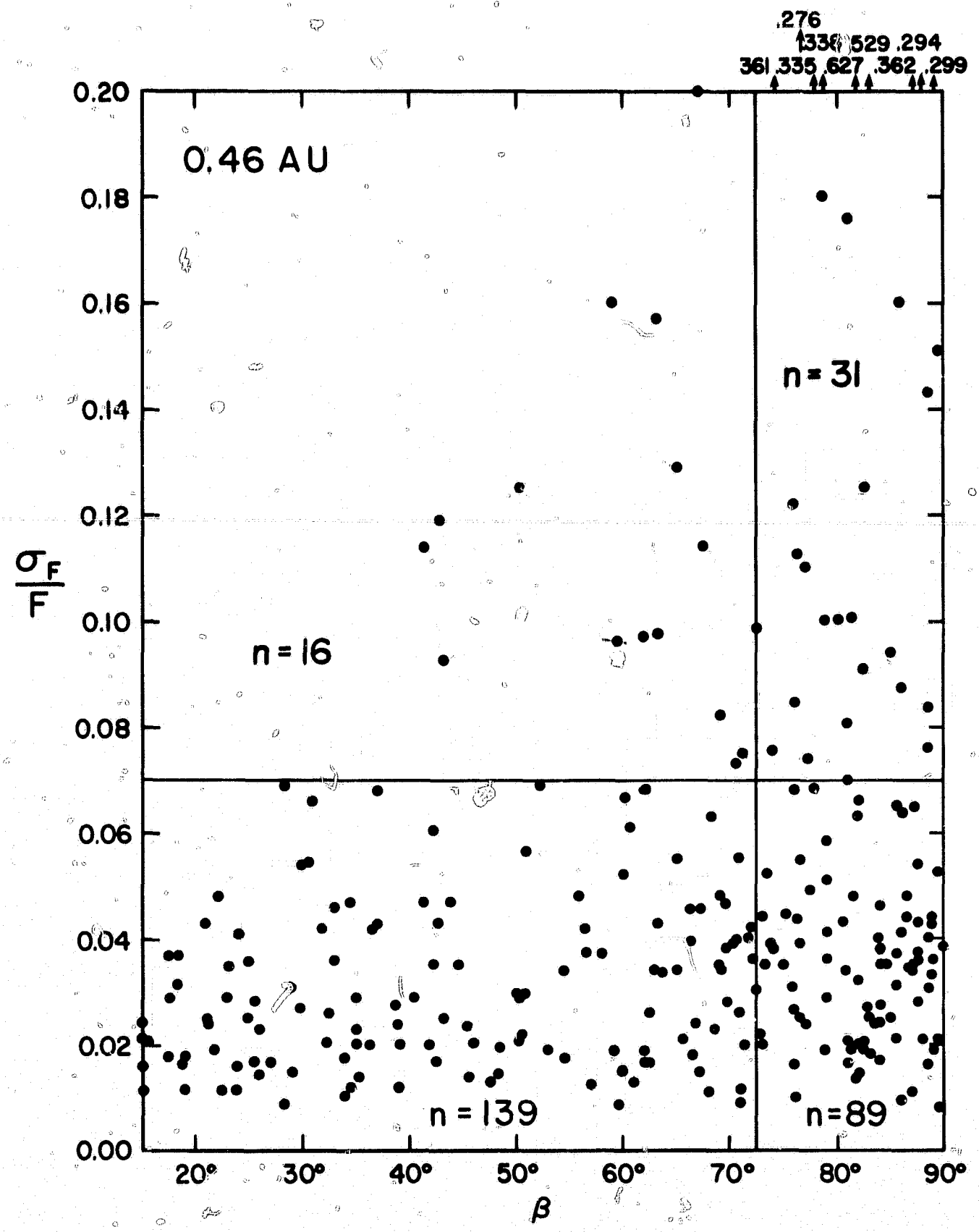
.276
.529 .294
361 .335 .627 .362 .299
0.46 AU
n = 31
n = 16
n = 139
n = 89
0.20
0.18
0.16
0.14
0.12
0.10
0.08
0.06
0.04
0.02
0.00
σF/F
20°
30°
40°
50°
60°
70°
80°
90°
β

Figure 7

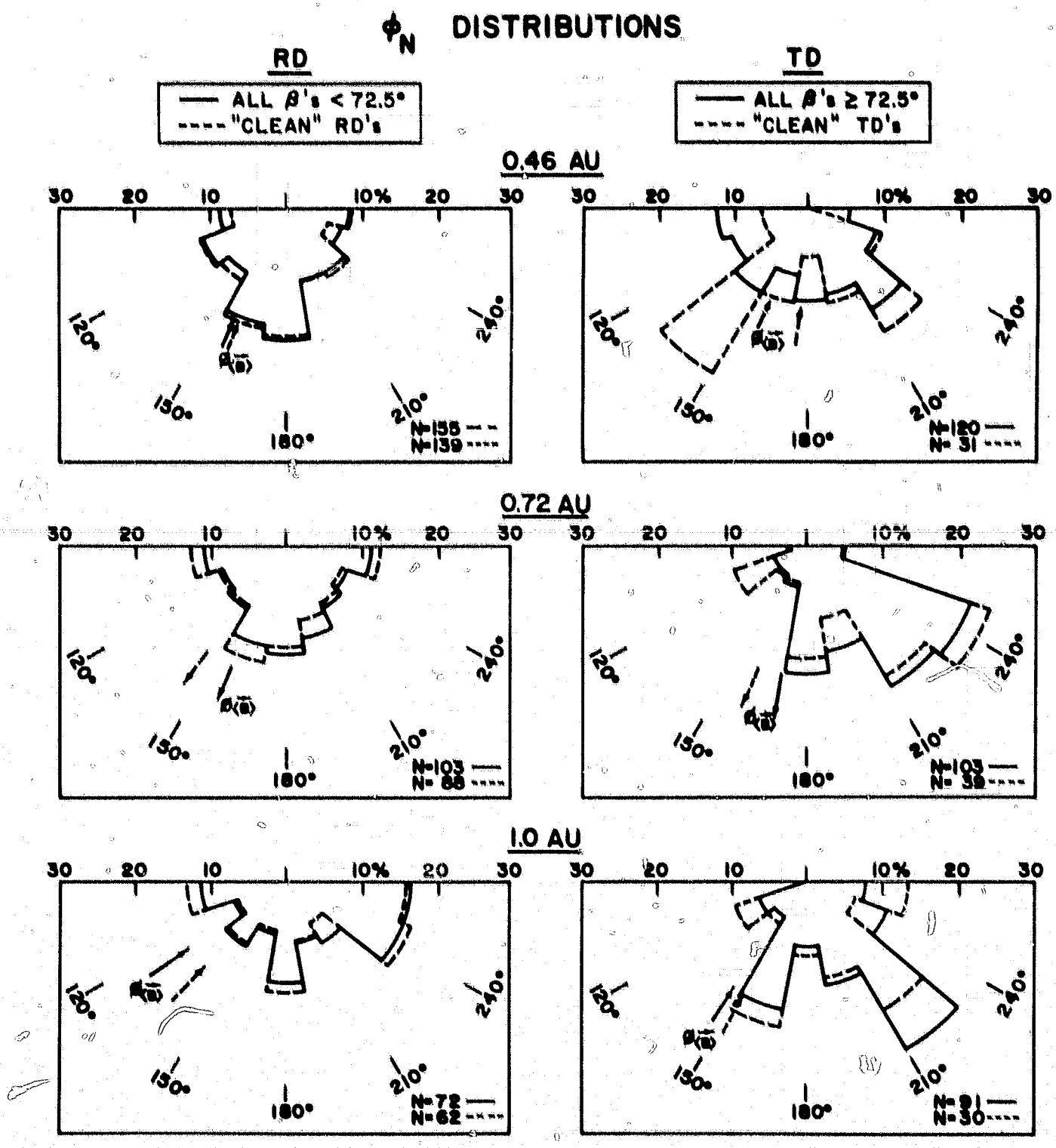
ϕ_N DISTRIBUTIONS
RD
— ALL β's < 72.5°
- - - - "CLEAN" RD's
TD
— ALL β's ≥ 72.5°
- - - - "CLEAN" TD's
0.46 AU
0.72 AU
1.0 AU
30 20 10 10% 20 30
120°
150°
180°
210°
240°
N=155 — —
N=139 - - - -
N=120 —
N= 31 - - - -
N=103 —
N= 88 - - - -
N=103 —
N= 39 - - - -
N=72 —
N=62 - - - -
N=91 —
N=30 - - - -

Figure 8

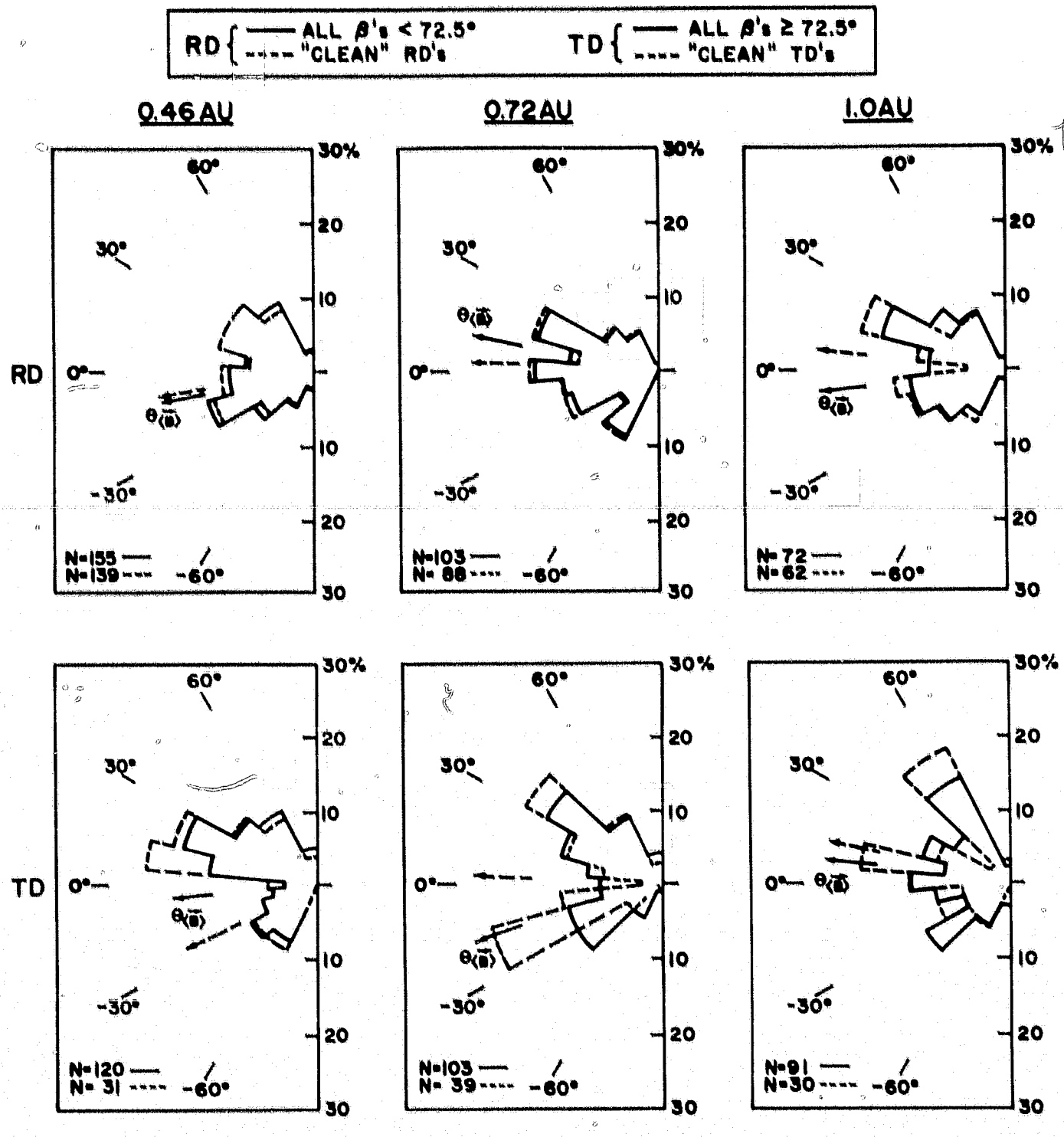
θN DISTRIBUTIONS
RD — ALL β's < 72.5°
RD ---- "CLEAN" RD's
TD — ALL β's ≥ 72.5°
TD ---- "CLEAN" TD's
0.46 AU
0.72 AU
1.0 AU
RD
TD
60°
30°
0°
-30°
-60°
30%
20
10
θ(B)
N=155 —
N=139 ---
N=103 —
N= 88 ----
N= 72 —
N= 62 ----
N=120 —
N= 31 ----
N=103 —
N= 39 ----
N=91 —
N=30 ----

Figure 9

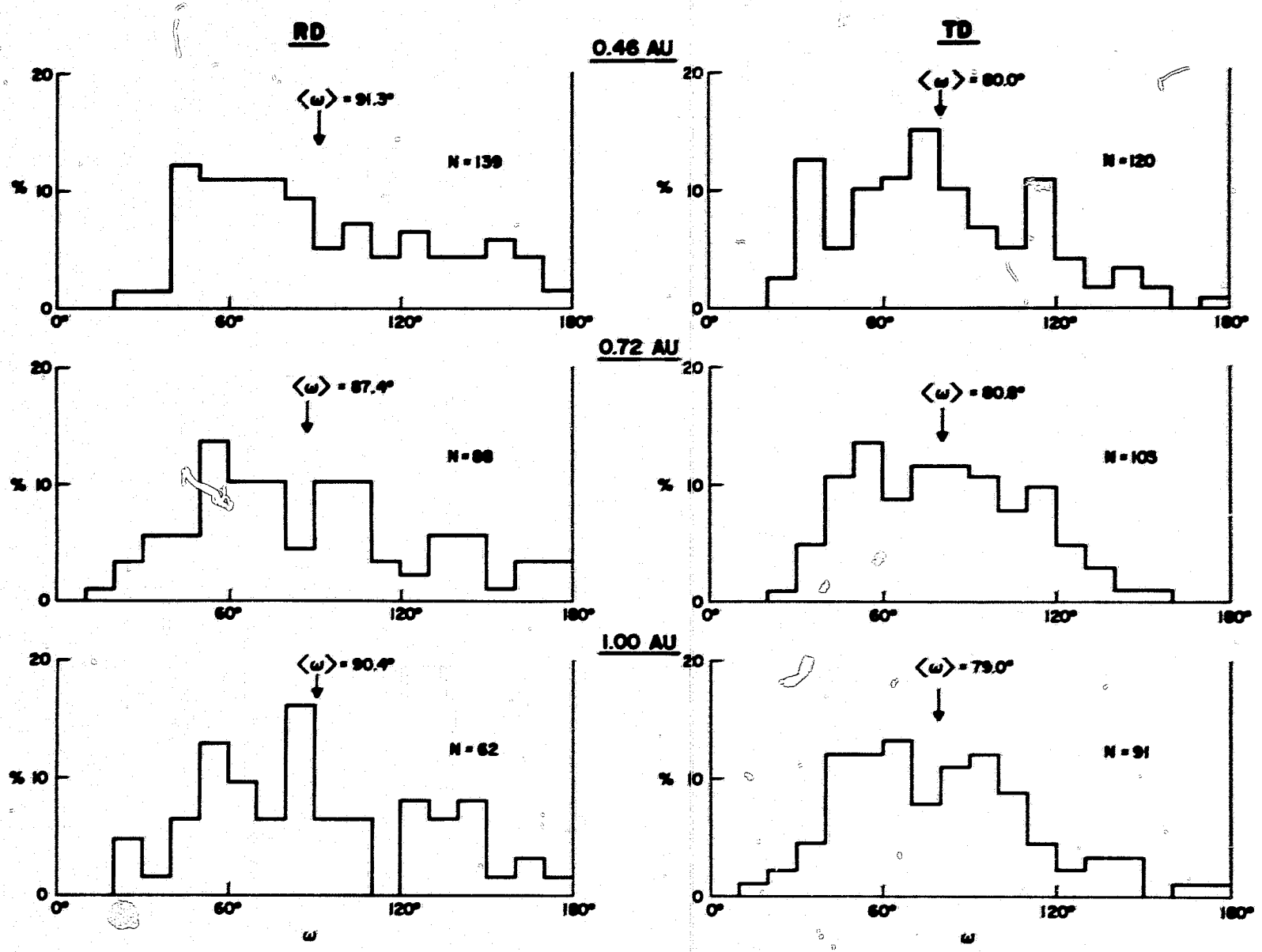
ω DISTRIBUTIONS
RD
TD
0.46 AU
⟨ω⟩ = 91.3°
N = 139
⟨ω⟩ = 80.0°
N = 120
0.72 AU
⟨ω⟩ = 87.4°
N = 88
⟨ω⟩ = 80.8°
N = 105
1.00 AU
⟨ω⟩ = 90.4°
N = 62
⟨ω⟩ = 79.0°
N = 91
%
20
10
0
0°
60°
120°
180°
ω

Figure 10

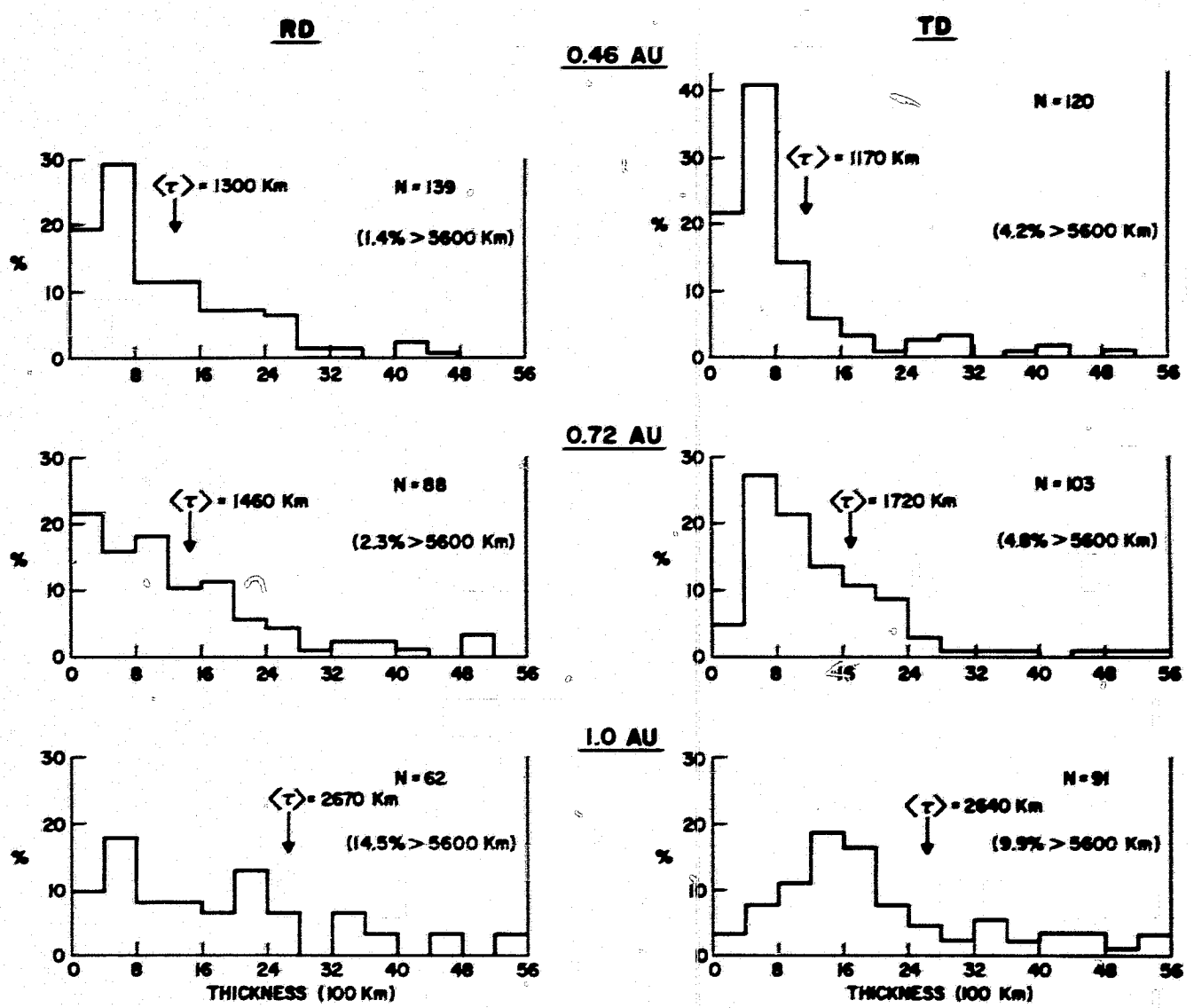
THICKNESS DISTRIBUTIONS
RD
TD
0.46 AU
⟨τ⟩ = 1300 Km
N = 139
(1.4% > 5600 Km)
⟨τ⟩ = 1170 Km
N = 120
(4.2% > 5600 Km)
0.72 AU
⟨τ⟩ = 1460 Km
N = 88
(2.3% > 5600 Km)
⟨τ⟩ = 1720 Km
N = 103
(4.8% > 5600 Km)
1.0 AU
⟨τ⟩ = 2670 Km
N = 62
(14.5% > 5600 Km)
⟨τ⟩ = 2640 Km
N = 91
(9.9% > 5600 Km)
%
THICKNESS (100 Km)

Figure 11

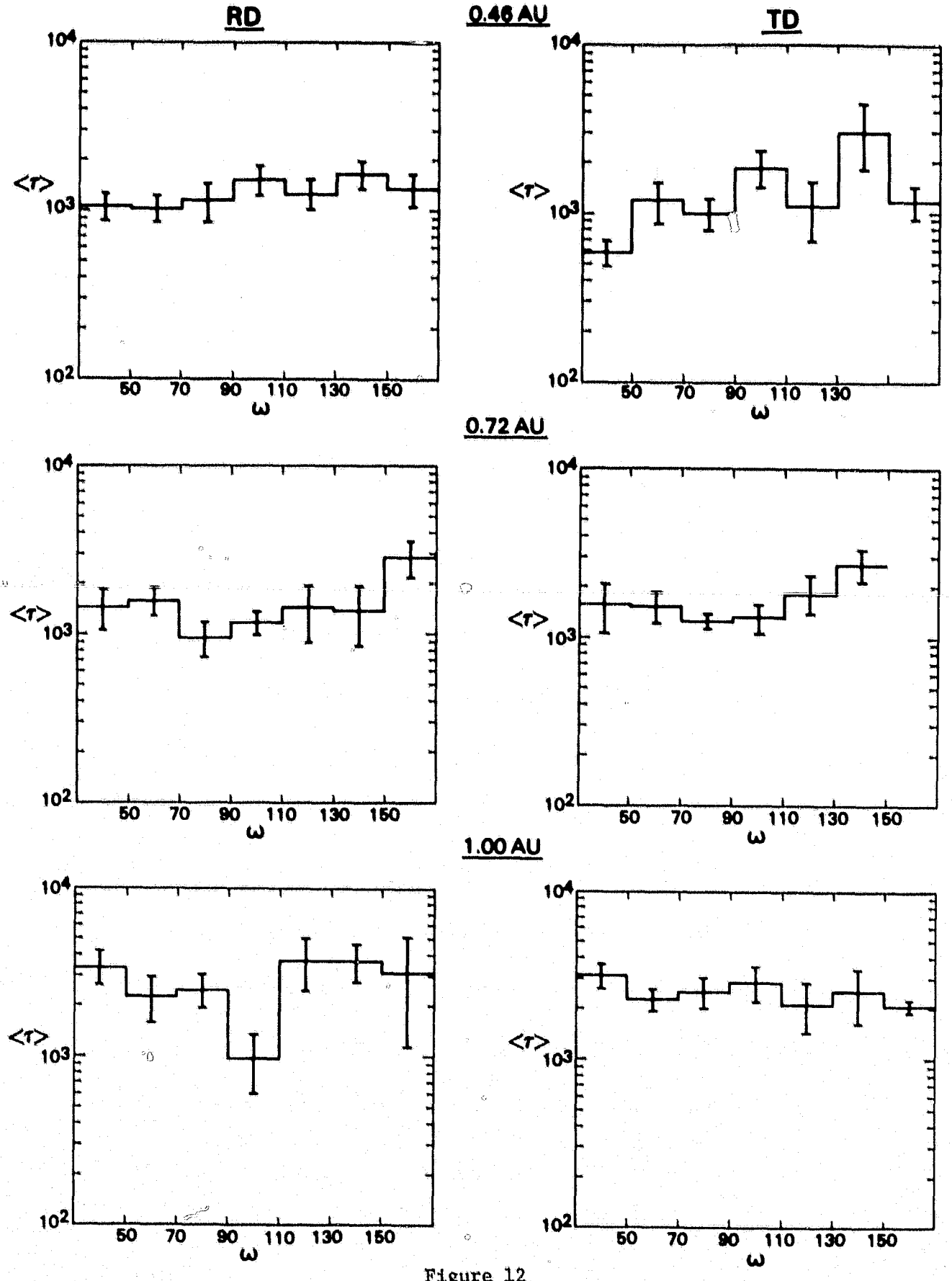

Figure 12